Validation of MODIS BRDF model parameters product and the Ross-Li model with POLDER data

ZHU Gaolong[1,2], JU Weimin[1], CHEN Jingming[1,3], LIU Yibo[1], ZHU Jingfang[1], XING Bailing[1]

1. *International Institute for Earth System Science*, *Nanjing University*, *Jiangsu Nanjing* 210093, *China*;
2. *Department of Geography*, *Minjiang University*, *Fujian Fuzhou* 350108, *China*;
3. *Department of Geography*, *University of Toronto*, *Toronto*, *Ontario*, M5S 3G3 *Canada*

Abstract: The ability of the RossThick-LiSparseR BRDF model (Ross-Li model) to simulate the bidirectional reflectance is assessed by comparing the reflectance simulated using the Ross-Li model based on the MCD43A1 data with the observed POLDER-3 BRDF data for 9961 pixels selected from the global POLDER-3/PARASOL BRDF archive. It is found that the Ross-Li model is able to simulate the bidirectional reflectance of ground objects efficiently. The R^2 and root mean square error (RMSE) of simulated reflectance are 0.934 and 0.016, respectively. On average, simulated reflectance is 5.2% lower compared with the POLDER-3 data. However, the Ross-Li model underestimates the reflectance by 14% for hotspots, with R^2 equal to 0.824 and RMSE equal to 0.07. The errors in simulated reflectance for hotspots depend on land cover types. Coniferous forests have the largest underestimates of simulated reflectance for hotspots, followed by broadleaved forests, grasslands, croplands, shrubs and barren lands. The modification for the volume kernel in the Ross-Li model can noticeably improve reflectance simulation for hotspots (R^2=0.839, RMSE=0.043).The reflectance simulated by the Ross-Li model is relatively accurate at nadir and darkspot. The departure of simulated reflectance from the POLDER-3 observations increases with the increases in solar zenith and view zenith angles. For grasslands and croplands, the accuracy of simulated reflectance decreases with the increase in NDVI. However, for forests and shrubs, the discrepancy between reflectance simulated by the Ross-Li model and the POLDER-3 observations maximizes when NDVI approximately equals 0.5.

Key words: MODIS, POLDER, hotspot reflectance, Ross-Li model, BRDF model parameters product

CLC number: TP702 **Document code:** A

Citation format: Zhu G L, Ju W M, Chen J M, Liu Y B, Zhu J F and Xing B L. 2011. Validation of MODIS BRDF model parameters product and the Ross-Li model with POLDER data. *Journal of Remote Sensing*, **15**(5): 875–894

1 INTRODUCTION

The bidirectional reflectance distribution function (BRDF) describes the anisotropy of surface reflectance as a function of sun and view angles (Nicodemus, *et al*., 1977). Directional spectra provided by BRDF are helpful for retrieving the structural parameters of surface targets. With the increasing availability of sensors able to provide multi-angle observation, such as Polarization and Directionality of Earth Reflectance (POLDER) and Multi-angle Imaging Spectroradiometer (MISR), BRDF has been paid more and more attentions and widely used in quantitative remote sensing, including the applications in albedo retrieval (Wanner, *et al*., 1997; Schaaf, *et al*., 2002), normalization of the geometry of remote sensing data acquired in different time (Leroy & Roujean, 1994; Wu, *et al*., 1995), land cover classification and retrieval of structural parameters of vegetation canopy such as leaf area index (LAI) and foliage clumping index based on spectra of specific directions (such as hotspot, darkspot, nadir, principle plain, and perpendicular plain) or various angular indices combined by the BRDF model parameters (Sandmeier & Deering, 1999; Gao, *et al*., 2003, Chen, *et al*., 2005).

POLDER and MISR are currently available two sensors able to observe BRDF data globally. But the POLDER data don't satisfy the requirements of global change study due to their low spatial resolution (about 6 km). While the spatial resolution of MISR data is relatively high (275 m in "Local Mode" and 1.1 km in "Global Mode"), the sensor is difficult to capture the reflectance of hotspot and darkspot due to its narrow swath width. MODIS (Moderate resolution Imaging Spectroradiometer) BRDF model parameters product is generated through fitting the MODIS observation data in 16 days with the RossThick-LiSparseR model (Ross-Li model)

Received: 2010-07-11; **Accepted**: 2010-11-16

Foundation: National High Technology Research and Development Program of China (863 program)(No. 2009AA12Z134); National Nature Science Foundation of China (No. 40871240; No. D011004); Open Funds of State Key Laboratory of Remote Sensing Science (No. 2009KFJJ014)

First author biography: ZHU Gaolong (1974—), male, associate professor, Ph.D. His research interest is retrieving biophysical parameters of vegetation covers using multi-angle remote sensing data. E-mail: zhugaolong@163.com

Corresponding author biography: JU Weimin (1963—), male, professor, his research interests are ecology environmental remote sensing and global change. E-mail: juweimin@nju.edu.cn

(Roujean, *et al*., 1992; Wanner, *et al*., 1995; Lucht, *et al*., 2000) and provides a new way for studying the surface reflectance anisotropy. However, this product tends to underestimate the reflectance of hotspot (Chen & Cihlar, 1997; Bréon, *et al*., 2002; Maignan, *et al*., 2004). Many studies have been conducted to validate the products of MODIS BRDF and albedo (Hu, *et al*., 1997; Liang, *et al*., 2002; Jiao, *et al*., 2005; Liu, *et al*., 2009). A commonly used method to assess the quality of MODIS BRDF parameters product is to conduct field observations at representative sites. This method is labor and time consuming and expensive. The observed site-level data cannot be directly used to validate the moderate resolution MODIS BRDF model parameters product.

It is one possible strategy to validate a BRDF product through the comparison of BRDF measurements from different spaceborne or airborne sensors on a homogeneity landscape (Hautecoeur & Leroy, 2000). Chen, *et al*. (2009) investigated the reflectance extrapolation ability of MISR and MODIS BRDF model parameters products through comparison of reflectance measured by MISR and MODIS with the reflectance calculated according to their BRDF model parameter products. However, this type of comparison is almost impossible to evaluate the accuracy of the hotspot reflectance simulated by MODIS BRDF model parameters product, since it is difficult for MISR to observe the reflectance along the principal plane. The reflectance of hotspot and darkspot is necessary for retrieving some structural parameters of vegetation canopy such as foliage clumping index and LAI. So it is necessary to assess the abilities of MODIS BRDF model parameters product and the Ross-Li model in simulating reflectance of hotspot and darkspot. This study takes the advantage of the POLDER sensor with more opportunities to acquire reflectance of hotspot and darkspot to evaluate the abilities of MODIS BRDF model parameters product and the Ross-Li model in estimating reflectance under different angular conditions. The influences of land cover types and vegetation density on errors of reflectance simulated by MODIS BRDF model parameters product and the Ross-Li model will also be analyzed.

2 MATERIALS AND METHODS

2.1 POLDER-3 BRDF product

The POLDER-3 sensor is onboard the PARASOL satellite. It uses a rotating CCD array as the detector to observe the global at daily time steps. The nadir spatial resolution is 6 km ×7 km. The maximum angle of view is 114°. The view zenith angles along and across the track can reach ± 61° and ± 50°, respectively, owing to Earth curvature. This sensor acquires multi-angle data through overlapping of field angle. It can observe a target from 16 different view angles in one overpass. The orbit shift causes changes in observation angles. If the weather condition is favorable, the POLDER-3 sensor can provide observations of almost full azimuth range for a surface target in a few of continuous days. POLDER-3 acquires the surface reflectance in 9 visible and near infrared (NIR) wavelengths, including 3 polarization bands. The surface reflectance at a resolution of 6.17 km is generated from the raw POLDER-3 multi-angle data through radiometric, geometric correction, cloud removal, atmospheric correction. The Laboratoire des Sciences du Climat et de l’Environnement (LSCE) selected surface reflectance with the best quality from the POLDER-3 data to build four annual and monthly global BRDF databases based on the IGBP and GLC2000 classification systems. The percentage of thematic homogeneity within each pixel is higher or equal to 80% for these four databases. The global monthly POLDER-3 BRDF database based on the GLC2000 land cover map is used in this study. There are totally 20985 pixels in this database with data acquired between November 2005 and October 2006. These pixels distributed globally and their land cover types are diverse, including all GLC2000 land cover types. The data of each pixel consist of the pixel directional observations acquired in a month, which are stored in the ASCII format, including the latitude, longitude, GLC2000 land cover type, NDVI, degree of homogeneity, date of observation, solar zenith angle (in degree), view zenith angle (in degree), relative azimuth angle (in degree), and surface reflectance of each band (Fig. 1). The observations from different angles for a pixel can reach 300 in a month, meaning that the POLDER-3 data cover almost full ranges of azimuth and view zenith angles (Fig. 2).

latitude	longitude	GLC2000_class	NDVI	nb_orbit	nb_dir	homogeneity(%)
25.69	99.71	4	0.45	6	84	85.71

yymmdd	thetaS	thetaV	RelAzi	R490	R565	R670	R765	R865	R1020
060201	44.97	58.67	37.06	0.062	0.090	0.104	0.225	0.266	0.325
060201	44.97	53.63	38.07	0.064	0.089	0.101	0.221	0.265	0.320
060201	44.97	47.62	39.47	0.063	0.088	0.101	0.214	0.256	0.312
060201	44.97	40.41	41.55	0.056	0.078	0.105	0.205	0.250	0.304
060201	44.97	31.86	45.04	0.048	0.070	0.088	0.190	0.229	0.280
060201	44.97	22.02	52.13	0.040	0.063	0.079	0.172	0.210	0.260
060201	44.97	11.92	72.89	0.040	0.060	0.080	0.158	0.191	0.243
060201	44.97	8.48	145.03	0.036	0.055	0.071	0.143	0.173	0.220
060201	44.97	17.16	185.79	0.031	0.049	0.059	0.128	0.157	0.199
060201	44.97	27.35	196.82	0.028	0.042	0.057	0.120	0.148	0.188
060201	44.97	36.53	201.53	0.028	0.041	0.054	0.115	0.143	0.179
060201	44.97	44.34	204.13	0.027	0.039	0.050	0.111	0.136	0.176
060201	44.97	50.88	205.78	0.028	0.039	0.047	0.106	0.133	0.169
060201	44.97	56.34	206.93	0.027	0.036	0.044	0.109	0.133	0.167
060203	43.59	60.70	52.07	0.051	0.073	0.086	0.191	0.232	0.282
060203	43.59	56.47	55.74	0.047	0.071	0.087	0.186	0.226	0.273

…………………………………

Fig. 1 The POLDER-3 BRDF data file of a pixel in ASCII format (latitude / (°); longitude / (°); nb_orbit: number of orbits; nb_dir: number of observations; yymmdd: date of the observation; thetaS: sun zenith angle / (°); thetaV: view zenith angle / (°); RelAzi: relative azimuth angle / (°); R490, R565, R670, R765, R865, R1020: surface reflectance measured at each band / nm)

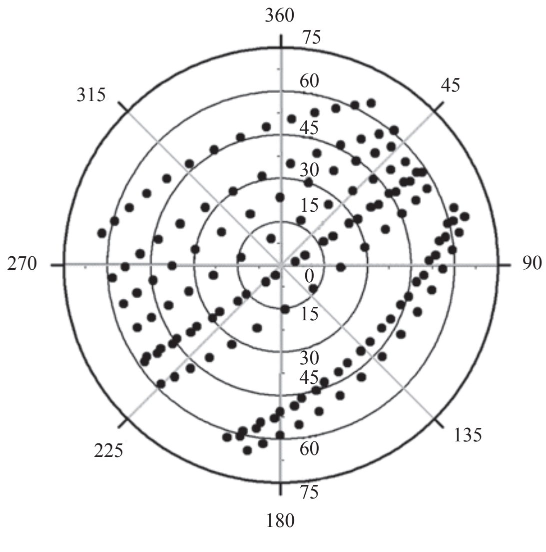

Fig. 2 The distribution of observation angles for a POLDER-3 pixel (The polar angle represents relative azimuth angle / (°), and the radius represents view zenith angle / (°))

2.2 MODIS BRDF model parameters product

The MODIS BRDF model parameters product (MCD43A1) is generated every 8 days through fitting the reflectance of MODIS onboard Terra and Aqua in 16 consecutive days using the Ross-Li model. The spatial resolution of this data is 463.3 m. The operational MODIS BRDF/Albedo algorithm used to generate MODIS BRDF model parameters product is on the basis of the kernel-driven RossThick-LiSparseR BRDF model (named as Ross-Li model for convenience) (Roujean, *et al*., 1992; Wanner, *et al*., 1995; Lucht, *et al*., 2000). The model uses the liner combinations of scattering kernels with physics meaning to simulate surface bi-directional reflectance. The present operational algorithm (version5) using the RossThick and LiSparseR kernels, which are expressed as:

$$R(\theta,\vartheta,\varphi)=f_{iso}+f_{vol}K_{vol}(\theta,\vartheta,\varphi)+f_{geo}K_{geo}(\theta,\vartheta,\varphi) \quad (1)$$

$$K_{vol}(\theta,\vartheta,\varphi)=\frac{(\pi/2-\xi)\cos\xi+\sin\xi}{\cos\theta+\cos\vartheta}-\frac{\pi}{4} \quad (2)$$

$$K_{geo}(\theta,\vartheta,\varphi)=O(\theta,\vartheta,\varphi)-\sec\theta-\sec\vartheta+\frac{1}{2}(1+\cos\xi)\sec\theta\sec\vartheta \quad (3)$$

$$O(\theta,\vartheta,\varphi)=\frac{1}{\pi}(t-\sin t\cos t)(\sec\theta+\sec\vartheta) \quad (4)$$

$$\cos t=2\frac{\sqrt{D^2+(\tan\theta\tan\vartheta\sin\phi)^2}}{\sec\theta+\sec\vartheta} \quad (5)$$

$$D=\sqrt{\tan^2\theta+\tan^2\vartheta-2\tan\theta\tan\vartheta\cos\varphi} \quad (6)$$

$$\cos\xi=\cos\theta\cos\vartheta+\sin\theta\sin\vartheta\cos\varphi \quad (7)$$

where $R(\theta,\vartheta,\varphi)$ is the bidirectional reflectance; θ, ϑ, and φ are the solar zenith angle, view zenith angle and relative azimuth angles, respectively; $K_{geo}(\theta,\vartheta,\varphi)$ and $K_{vol}(\theta,\vartheta,\varphi)$ are the geometric optical kernel (LiSparseR kernel) and volumetric scattering kernel (RossThick kernel), both depending only on θ, ϑ, and φ; ξ is the scattering angle, namely, the angle between the sensor and the sun relative to the target; f_{iso}, f_{vol}, and f_{geo} are the weight parameters for the isotropic, geometric and volumetric kernels, respectively.

The operational MODIS BRDF/Albedo algorithm employs the least squares method to derive f_{iso}, f_{vol}, and f_{geo} for users as MODIS BRDF model parameters product according to $R(\theta,\vartheta,\varphi)$ acquired from different angles in 16 consecutive days and corresponding $K_{geo}(\theta,\vartheta,\varphi)$ and $K_{vol}(\theta,\vartheta,\varphi)$ calculated using Eqs. (2) (3). Parameters f_{iso}, f_{vol}, and f_{geo} can be used in conjunction with Eqs. (1)—(7) to simulate the bidirectional reflectance at any desired illumination and view angles.

2.3 Data preparation and processing

The ability of MODIS BRDF model parameters product to extrapolate reflectance at any angles is validated using POLDER-3 BRDF product. According to the acquisition time, 1193 tiles of MCD43A1 and corresponding quality product (MCD43A2) were downloaded from LP DAAC (Land Processes Distributed Active Archive Center). There are certain numbers of POLDER-3 pixels with BRDF data available in each tile of MODIS data. The downloaded globally distributed MCD43A1 data were acquired during the period from November, 2005 to October, 2006, covering most cover types and various vegetation densities. In this study, we just assess the ability of MODIS BRDF model parameters product in extrapolating the bidirectional reflectance in the NIR band, which is usually used to retrieve the foliage clumping index. The NIR channel of MODIS, which covers a spectral domain ranging from 841 nm to 876 nm, is comparable with that of POLDER-3 with a center wavelength of 865 nm and a bandwidth of 40 nm.

2.3.1 Spatial match of MODIS and POLDER pixels

The reference grids of POLDER-3 and MCD43A1 are both centered on the Greenwich meridian with the same sinusoidal equal area projection. There are 3240×6480 pixels in the global POLDER-3 reference grid. MCD43A1 uses the sinusoidal grid tiling system. There are 18×36 tiles in the global total. Each MCD43A1 tile consists of 2400×2400 pixels. So the size of a POLDER-3 pixel is approximately equal to that of 13×13 MCD43A1 pixels. The following equations are used to determine the positions of the 169 MCD43A1 pixels in the MCD43A1 reference grid corresponding to a POLDER-3 pixel:

$$V=\mathrm{INT}((lin-1)/180) \quad (8)$$

$$H=\mathrm{INT}((col-1)/180) \quad (9)$$

$$r=\mathrm{INT}(40/3\times\mathrm{MOD}((lin-1),180)) \quad (10)$$

$$p=\mathrm{INT}(40/3\times\mathrm{MOD}((col-1),180)) \quad (11)$$

where *lin* and *col* are the line and column numbers of the POLDER-3 pixel in the POLDER-3 reference grid, respectively; V and H are the horizontal and vertical tile numbers of the 169 MCD43A1 pixels in the MCD43A1 tile coordinate system, respectively; r and p are the row and column numbers of the upper left corner pixel within the 169 MCD43A1 pixels in the above tile, respectively; INT is the function rounds a number to the nearest integer, and MOD stands for the modular arithmetic.

2.3.2 Data processing

Firstly, the169 MCD43A1 pixels and their retrieval quality (MCD43A2) corresponding to a POLDER-3 BRDF pixel are extracted using the above equations (Eqs. (8)—(11)). If the data of 169 MCD43A1 pixels are all in the best or good quality (MODIS QA=0 or 1), the bidirectional reflectance in the NIR band of these pixels is simulated using Eq. (1) (the Ross-Li model) based on parameters from MCD43A1 data and the solar zenith, view zenith, and relative azimuth angles from the POLDER-3 BRDF data. Then, the mean value of the bidirectional reflectance of the 169 MODIS pixels is compared with the reflectance observed by POLDER-3 instrument to evaluate the ability of the Ross-Li model in conjunction with MODIS BRDF model parameters product to extrapolate bidirectional reflectance at given illumination and view angles. The sizes of POLDER-3 and MODIS pixels are considerably different. Since scaling effect of BRDF is linear (Liang, 2004) and the land cover types of the selected POLDER-3 pixels are almost homogenous (The coverage of a dominant cover in a POLDER-3 pixel is above 80%), the effects of scale difference between POLDER-3 and MODIS data on the evaluation results are not taken into account in this study.

3 RESULTS AND DISCUSSIONS

3.1 Processed data

The Ross-Li model is not applicable for some non-vegetation land cover types such as snow. In order to constrain the impact of non-vegetation pixels on the assessment results, only 9961 vegetation pixels with NDVI above 0.15 are further selected among

20985 POLDER-3 pixels for the assessment purpose. There are 19 land cover types of the GLC2000 classification system for these 9961 pixels, excluding the types of water bodies, snow and ice, and artificial surfaces. Table 1 summaries the information of the selected POLDER-3 pixels for each of 19 land cover types, including the pixel number, observation number, NDVI range and mean, range of solar zenith angle and average reflectance. The valid observations of a single POLDER-3 pixel vary from 6 to 199. The total observations of all the selected POLDER-3 pixels are 714652. On average, there are 72 observations for a POLDER-3 pixel during the period of 16 days in which corresponding MODIS BRDF model parameters product is generated. NDVI varies from 0.15 to 0.87 for all POLDER-3 pixels. Its range is considerably large for all land cover types. The solar zenith angles, view zenith angles, and relative azimuth angles vary from 11.4º to 74.7º, from 0.1º to 67.6º, and from 0º to360º for all 9961 POLDER-3 pixels, respectively.

Fig. 3 presents the comparison of 714652 observations at different angles by the POLDER-3 instrument with that simulated by the Ross-Li model. The Ross-Li model with MODIS BRDF model parameters product as input is able to simulate the bidirectional reflectance of ground objects efficiently. The coefficient of determination (R^2) and root mean square error (RMSE) of simulated reflectance are 0.934 and 0.016 for 714652 observations, respectively. Forests have the largest RMSE of simulated reflectance, followed by shrubs, croplands, grasslands, and barren lands. On average, simulated reflectance is 5.2% lower compared with the POLDER-3 data. Fig. 4 shows the comparison of the bidirectional reflectance along the principal plane ($0° \leqslant \varphi \leqslant 10° \cup 170° \leqslant \varphi \leqslant 190° \cup 350° \leqslant \varphi \leqslant 360°$) simulated by the Ross-Li model based on MCD43A1 BRDF parameters product with the POLDER-3 data of a needle-leaved pixel shown in Fig. 1. It is found that the Ross-Li model is able to reproduce reflectance in most cases. However, it considerably underestimates the hotspot reflectance.

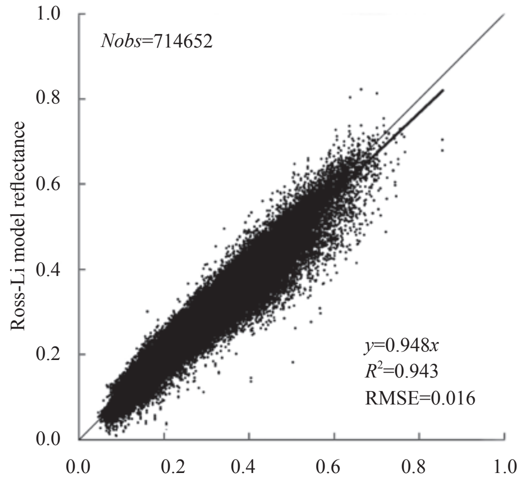

Fig. 3 The comparison of reflectance observed by POLDER-3 from different angles and that simulated by the Ross-Li model

Table 1 Statistics of the selected POLDER-3 data

GLC2000 land cover type	No. of Pixels	No. of observations	NDVI range	Mean NDVI	Solar zenith angle range / (°)	Mean reflectance of POLDER-3	Mean reflectance simulated by the Ross-Li model	RMSE
Broadleaved, evergreen	455	30370	0.29—0.84	0.71	15.4—66.2	0.256	0.251	0.020
Broadleaved, deciduous, closed	1002	78400	0.18—0.87	0.55	11.4—70.3	0.235	0.232	0.016
Broadleaved, deciduous, open	378	30110	0.20—0.79	0.43	17.4—62.3	0.213	0.209	0.014
Needle-leaved, evergreen	545	39452	0.17—0.86	0.51	12.0—74.7	0.202	0.208	0.017
Needle-leaved, deciduous	628	35762	0.15—0.81	0.56	28.6—72.8	0.221	0.215	0.018
Tree cover, mixed leaf type	569	35684	0.25—0.87	0.55	13.7—74.5	0.222	0.217	0.017
Tree cover, flooded, fresh	13	709	0.60—0.80	0.66	26.3—48.2	0.249	0.240	0.022
Tree cover, flooded, saline	58	4136	0.15—0.73	0.51	15.3—52.1	0.239	0.236	0.020
Mosaic: tree cover / other	720	41858	0.21—0.86	0.63	12.2—74.4	0.240	0.238	0.017
Tree cover, burnt	436	24405	0.24—0.81	0.55	28.3—74.7	0.216	0.212	0.017
Shrub cover, evergreen	802	52483	0.15—0.87	0.63	12.2—74.5	0.269	0.267	0.017
Shrub cover, deciduous	563	49367	0.15—0.73	0.32	11.5—74.6	0.224	0.221	0.013
Herbaceous, closed-open	732	60783	0.15—0.83	0.30	14.8—73.4	0.249	0.247	0.014
Sparse herbaceous or shrub	725	60016	0.15—0.64	0.27	15.7—72.6	0.251	0.248	0.013
Flooded shrub and herbaceous	568	39177	0.15—0.82	0.57	16.7—73.8	0.259	0.256	0.019
Cultivated and managed areas	700	59156	0.15—0.85	0.38	12.6—71.7	0.261	0.257	0.014
Mosaic: cropland / tree cover	453	27481	0.17—0.87	0.69	15.9—62.0	0.293	0.293	0.017
Mosaic: cropland / shrub	535	39580	0.15—0.79	0.41	14.7—73.6	0.272	0.270	0.015
Bare areas	79	5723	0.15—0.44	0.21	19.8—68.0	0.218	0.218	0.012
Total	9961	714652	0.15—0.87	0.50	11.4—74.7	0.244	0.241	0.016

3.2 The ability of the Ross-Li model to simulate hotspot reflectance and its improvement

If the illumination and view directions coincide, the areas observed by the senor are all illuminated while all shadows cannot be observed by the sensor. In this case, the sensor can observe strong peak reflectance. This phenomenon refers to hotspot. With the departure of view direction from illumination direction, the shaded areas observed by the sensor gradually increases, resulting in the rapid decrease of observed reflectance (Fig. 4). The underestimation of hotspot reflectance simulated by the Ross-Li model is caused by its hypotheses. The RossThick kernel (the volumetric kernel) of the Ross-Li model is derived from the radiative transfer model developed by Ross (1981), which is suitable for horizontally homogenous dense vegetation canopies and does not account for the probability of mutual shadowing within canopy (Roujean, *et al*., 1992). The LiSparseR kernel (the geometrical kernel) is derived from the Li-Strahler geometric optical (GO) model (Li & Strahler, 1985, 1986; Jiao, 2008), which is suitable for describing sparse vegetation canopies (Wanner, *et al*., 1997; Lucht, *et al*., 2000). The GO model assumes the shape of tree crown is an opaque lightproof sphere or ellipsoid. This model is actually a single scattering model (Xu, 2005). Although it consider the difference in sunlit crown, sunlit background, shaded crown, and shaded background under the condition of illumination by direct solar beam, it does not consider the shadows caused by the changes of gaps within the crown with illumination and view angles. Although the geometric optical kernel of the Ross-Li model has a peak value at the hotspot (Lucht, *et al*., 2000), this peak is not large enough to capture the hotspot signal. Therefore, the Ross-Li model is unable to quantify hotspot properly.

Based on the 4-scale model (Chen & Leblanc, 1997), Chen & Cihlar (1997) used two coefficients to correct the volumetric and geometrical scattering kernels in the kernel-based BRDF model. The two coefficients are used to correct the magnitude and width of hotspot. The modification significantly improved the simulation of hotspot reflectance by the kernel-based model. Maignan, *et al*. (2004) proposed a simple algorithm to improve the simulation of hotspot reflectance through only modifying the volumetric kernel (RossThick kernel), *i.e.*,

$$K_{vol}(\theta,\vartheta,\varphi)=\frac{(\pi/2-\xi)\cos\xi+\sin\xi}{\cos\theta+\cos\vartheta}\left(1+(1+\xi/\xi_0)^{-1}\right)-\frac{\pi}{4} \tag{12}$$

where ξ is the scattering angle calculated using Eq. (7); ξ_0 is the specific angle related to the ratio of scattering element size to the canopy vertical density and assigned a constant value of 1.5° here. The Maignan's method (named as Ross-Li-M model hereafter) is used to correct Ross-Li model in this study.

In order to validate the accuracy of hotspot reflectance simulated by the Ross-Li model, 5061 observations near hotspot are extracted from the above POLDER-3 BRDF dataset using the criteria of $0° \leqslant \varphi \leqslant 10° \cup 350° \leqslant \varphi \leqslant 360° \cap |\vartheta-\theta| \leqslant 2°$. Table 2 shows the linear regressions between the hotspot reflectance observed by POLDER-3 and that simulated by the Ross-Li model and the Ross-Li-M model for each cover type. In these regression models, intercept is forced to be zero with simulations and POLDER-3 data denoting y and x, respectively. For the reflectance simulated by the Ross-Li model, the slope values range from 0.806 to 0.916 and R^2 values are from 0.569 to 0.913, respectively. The RMSE values of simulated hotspot reflectance vary from 0.044 to 0.090. The departures of hotspot reflectance simulated by the Ross-Li model from the POLDER-3 data depend on land cover types. The discrepancy between the simulated hotspot reflectance and the POLDER-3 data is the largest for coniferous forests, with the largest underestimation of 18.6%, the smallest R^2 of 0.611 and the largest RMSE of 0.083. For broadleaved forests, the hotspot reflectance is underestimated by 16%, with R^2 and RMSE equal to 0.8 and 0.076, respectively. The hotspot reflectance of grasslands and croplands is underestimated by about 15% while R^2 values equal 0.803 and 0.843 and RMSE values equal 0.07 and 0.068 for these two land cover types, respectively. The underestimates in hotspot reflectance of shrubs and barren lands are 11% and 13%, respectively. Their R^2 values of simulated hotspot reflectance equal 0.868 and 0.803 and corresponding RMSE values equal 0.065 and 0.048, respectively. Among all cover types, the largest underestimation in the hotspot reflectance simulated by the Ross-Li model for coniferous forests may be caused by the more distinct canopy structure of coniferous forests, resulting in relatively greater hotspot effects. The relatively homogenous canopies of grasslands and croplands result in weaker hotspot phenomena. Consequently, the underestimation of their hotspot reflectance by the Ross-Li model is relatively small. The Ross-Li-M improved the simulations of hotspot reflectance for all cover types with the exception of cover type 15 (flooded shrub and herbaceous) (Table 2). It efficiently corrected the systematic underestimates of hotspot reflectance caused by the Ross-Li model.

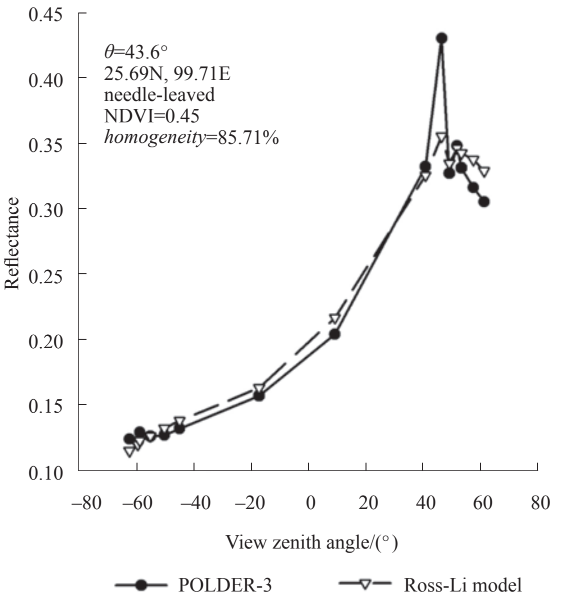

Fig. 4 Comparison of the bidirectional reflectance along the principle plane simulated by the Ross-Li model using MCD43A1 BRDF parameters with POLDER-3 data for a needle-leaved pixel shown in Fig.1 (The positive values in x-axis denote backward reflectance and negative values indicate forward reflectance)

Fig. 5 and Fig. 6 show the relationships between the 5061 hotspot reflectance observed by the POLDER-3 and those simulated by the Ross-Li model and the Ross-Li-M model, respectively. The slope of the regression model with intercept set as zero is 0.859

for the Ross-Li model while it increases to 1.028 for the Ross-Li-H model. The R^2 value of hotspot reflectance simulated by the Ross-Li-M is 0.839, slightly higher than the value of 0.824 resulted from simulations using the Ross-Li model. The RMSE value of hotspot reflectance simulated by the Ross-Li-M model equals 0.043 while it is 0.07 in the simulations using the Ross-Li model. The improvement on hotspot reflectance by the Ross-Li-M model is more outstanding for high hotspot reflectance. As to the reflectance simulations for all 714652 POLDER-3 observations, the Ross-Li-M model also surpassed the Ross-Li model, indicated by the increases in the slope of the regression model and R^2 value from 0.948 and 0.943 for the Ross-Li model to 1.027 and 0.967 for the Ross-Li-M model, respectively, and the corresponding decrease of RMSE from 0.016 to 0.015 (Fig. 3 and Fig. 7).

Table 2　Comparison of the results of the hotspot reflectance simulated by the Ross-Li model and Ross-Li-M model

GLC2000 land cover type	No. of observ-ations	Mean NDVI	Ross-Li model			Ross-Li-M model		
			Regression equation	R^2	RMSE	Regression equation	R^2	RMSE
Broadleaved, evergreen	243	0.72	y=0.859x	0.824	0.090	y=1.028x	0.839	0.044
Broadleaved, deciduous, closed	558	0.54	y=0.852x	0.742	0.072	y=1.017x	0.814	0.036
Broadleaved, deciduous, open	211	0.43	y=0.815x	0.689	0.071	y=1.009x	0.840	0.027
Needle-leaved, evergreen	285	0.54	y=0.820x	0.638	0.081	y=0.983x	0.800	0.034
Needle-leaved, deciduous	244	0.60	y=0.806x	0.569	0.085	y=0.971x	0.795	0.037
Tree cover, mixed leaf type	237	0.55	y=0.840x	0.606	0.077	y=0.993x	0.811	0.033
Tree cover, flooded, fresh	8	0.68	y=0.855x	0.913	0.063	y=1.020x	0.797	0.031
Tree cover, flooded, saline	14	0.45	y=0.908x	0.886	0.044	y=1.037x	0.818	0.041
Mosaic: tree cover / other	317	0.64	y=0.888x	0.859	0.068	y=1.020x	0.897	0.041
Tree cover, burnt	209	0.52	y=0.827x	0.634	0.069	y=0.978x	0.822	0.028
Shrub cover, evergreen	379	0.60	y=0.916x	0.828	0.065	y=1.047x	0.856	0.054
Shrub cover, deciduous	307	0.33	y=0.844x	0.834	0.064	y=1.045x	0.847	0.038
Herbaceous, closed-open	416	0.30	y=0.847x	0.803	0.070	y=1.034x	0.778	0.043
Sparse herbaceous or shrub	487	0.27	y=0.857x	0.799	0.062	y=1.046x	0.804	0.038
Flooded shrub and herbaceous	257	0.58	y=0.881x	0.740	0.061	y=1.124x	0.553	0.083
Cultivated and managed areas	398	0.39	y=0.852x	0.843	0.068	y=1.041x	0.864	0.037
Mosaic: cropland / tree cover	204	0.66	y=0.908x	0.817	0.064	y=1.041x	0.876	0.043
Mosaic: cropland / shrub	247	0.40	y=0.853x	0.862	0.067	y=1.064x	0.882	0.043
Bare areas	40	0.21	y=0.873x	0.803	0.048	y=1.056x	0.891	0.028
Total	5061	0.48	y=0.859x	0.824	0.070	y=1.028x	0.839	0.043

Note: x is the reflectance in NIR band measured by POLDER-3, y is the corresponding reflectance simulated by the Ross-Li model or the Ross-Li-M model

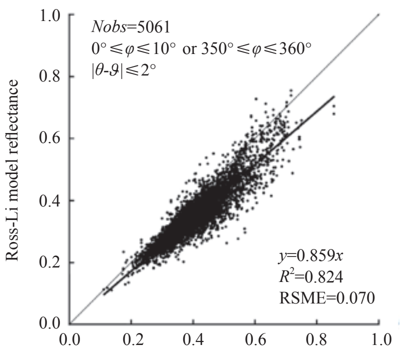

Fig. 5　Comparison of hotspot reflectance observed by the POLDER-3 with that simulated using the Ross-Li model

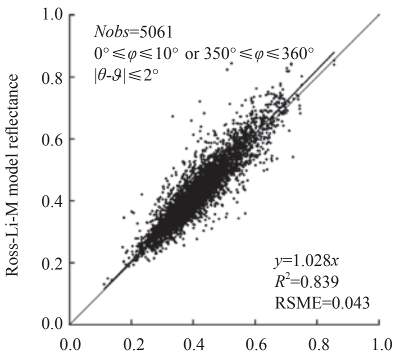

Fig. 6　Comparison of hotspot reflectance observed by the POLDER-3 with that simulated using the Ross-Li-M model

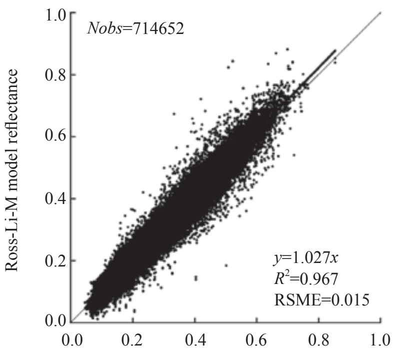

Fig. 7　Comparison of all reflectance observed by the POLDER-3 with that simulated using the Ross-Li-M model

3.3　The effects of solar and view zenith angles on reflectance simulated by the Ross-Li model

The errors in hotspot reflectance simulated by the Ross-Li model are quite large. In order to assess the sensitivity of reflectance simulated by the Ross-Li model to solar zeniths and view zenith angles, observations in the POLDER-3 BRDF dataset very close to hotspot are excluded, resulting in 709591 observations. All the 709591 selected POLDER-3 observations and corresponding simulated reflectance values are binned at 1 degree intervals of solar zenith angle, respectively. The R^2 and RMSE values are calculated for each solar zenith angle interval using the POLDER-3 data as the benchmarks to assess the change of errors in reflectance simulated by the Ross-Li model with solar zenith angle. With the increase in solar zenith angle, the R^2 values generally decrease while the RMSE values generally increase. The RMSE values are above 0.02 for solar zenith angles above 65º (Fig. 8). The relation of errors in simulated reflectance by the Ross-Li model with view zenith angles is also analyzed in the same way. The increases of view zenith angle cause R^2 to decrease and RMSE to increase (Fig. 9). Overall, these results are in agreement with previous findings by Chen, *et al*. (2009). The RMSE values are larger than 0.02 if the view zenith angles are above 63º. The errors in reflectance simulated by the Ross-Li model are more sensitive to solar zenith angle than to the view zenith angle.

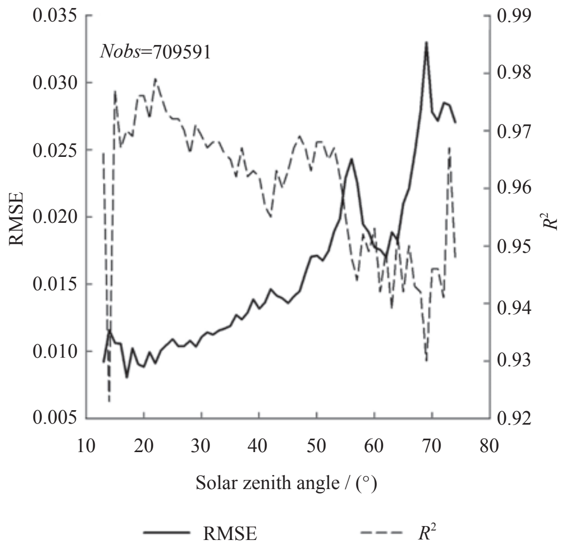

Fig. 8 Changes in the accuracy of reflectance simulated by the Ross-Li model with solar zenith angles

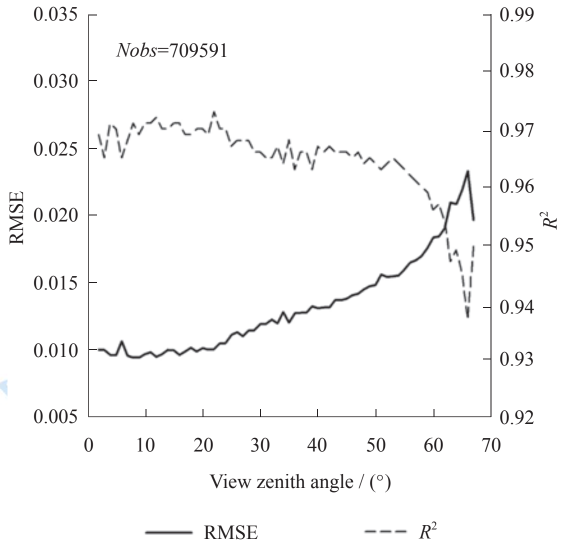

Fig. 9 Changes in the accuracy of reflectance simulated by the Ross-Li model with view zenith angles

The large errors in simulated reflectance for large view zenith angles are related to the LiSparseR kernel used in the Ross-Li model. The LiSparseR kernel is the modified LiSparse kernel which was developed based on the reciprocal theory. The LiSparse kernel assumes that the total area of vegetation and shadows is much smaller than the total area of view field. The ratio of these two areas is approximately positively proportional to sec (ϑ) (Yang, *et al*., 2002). In the case of large view zenith angles, the above assumption fails and simulated reflectance will have very large errors, even negative values. Although LiSparseR kernel can remedy this problem to some extent, it still fails to remove the influences of large view zenith angles. LiSparseR kernel assumes that the solar zenith angle is reciprocal with view zenith angle (Wanner, *et al*., 1995, Wanner, *et al*., 1997; Lucht, *et al*., 2000). The effects of solar zenith angle on simulated reflectance by the Ross-Li model are similar to those of view zenith angle. Li & Wan (1998) pointed out that the application of reciprocal principle as the prerequisite for the construction of the BRDF models is not theoretically solid. This issue is not discussed in this paper.

In the classification of vegetation types and retrieval of vegetation structure parameters, nadir reflectance and darkspot reflectance is usually required. Therefore, the accuracy of reflectance at these directions simulated by the Ross-Li model is assessed with the POLDER-3 observed data, which are chosen according to the following criteria, $\vartheta \leqslant 10°$ for the nadir observations and $45° \leqslant \vartheta \leqslant 50° \cup 170° \leqslant \varphi \leqslant 190°$ for the darkspot observations. The reflectance simulated by the Ross-Li model is closer to the observations of POLDER-3 at nadir and darkspot directions (Fig. 10 and Fig. 11). The R^2 values are 0.968 and 0.947 for nadir and darkspot directions, respectively. The corresponding RMSE values are 0.01 and 0.011.

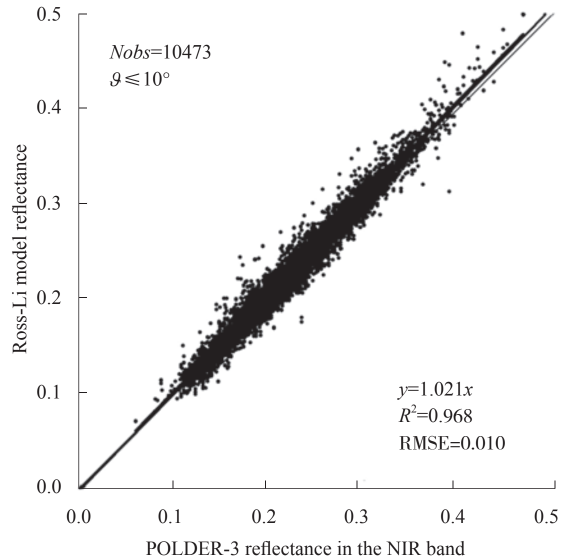

Fig. 10 Comparison of the nadir reflectance observed by the POLDER-3 against the simulations by the Ross-Li model

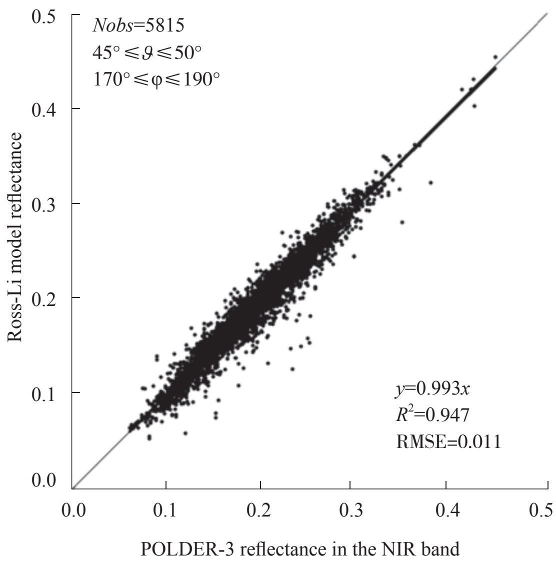

Fig. 11 Comparison of the darkspot reflectance observed by the POLDER-3 against the simulations by the Ross-Li model

3.4 The influence of NDVI on the ability of the Ross-Li model to extrapolate reflectance

The changes in the agreement of reflectance simulated by the Ross-Li model with the POLDER-3 BRDF data with NDVI are analyzed for five dominant cover types, including "broadleaved, deciduous, closed", "needle-leaved, deciduous", "shrub cover, evergreen", "herbaceous, closed-open", and "cultivated and managed areas". For each selected cover type, the simulated reflectance and POLDER-3 data are binned at 0.1 intervals of NDVI. The R^2 and RMSE of simulated reflectance are calculated for every NDVI interval (Fig. 12 and Fig. 13). The R^2 and RMSE values of all cover types considerably vary with the NDVI. With an increase in NDVI, the RMSE values of simulated reflectance of grasslands and croplands increase while the R^2 values decrease. For the remaining three cover types, the discrepancy between reflectance simulated by the Ross-Li model and the POLDER-3 observations maximizes when vegetation density is medium (NDVI approximately equals to 0.5). Forests and shrubs have more distinct canopy structure than grasslands and croplands. The shadow effects of forests and shrubs maximize when NDVI is medium owning to the low probability of shadows being overlaid for sparse discrete vegetations. Consequently, the hotspot is obvious in this case, resulting in the maximum RMSE values and the minimum R^2 values for forests and shrubs.

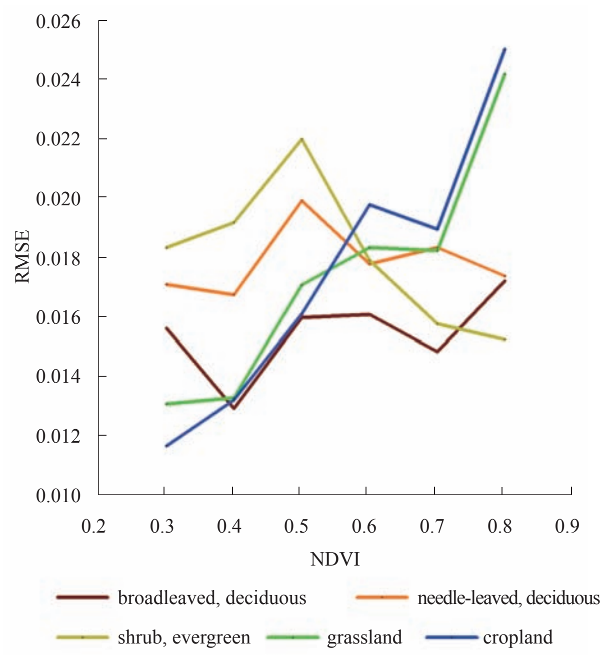

Fig. 12 Changes in the RMSE values of the reflectance simulated by the Ross-Li model with NDVI for 5 cover types. In the calculation of RMSE, simulated and observed reflectance is binned at 0.1 interval of NDVI

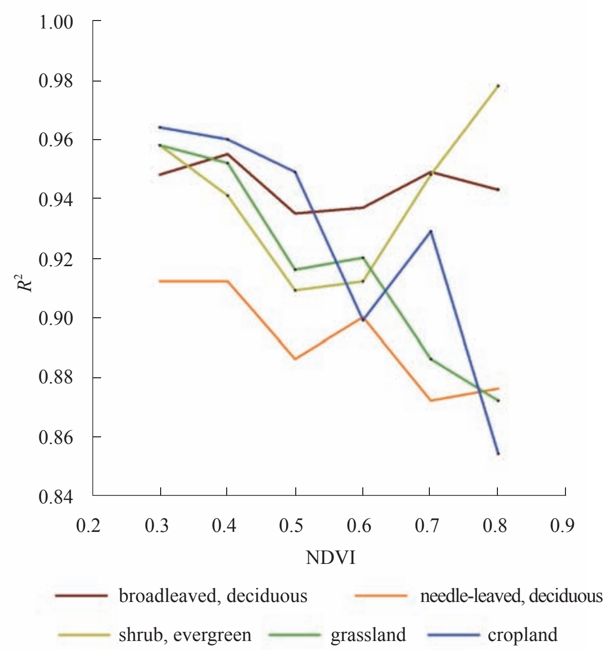

Fig. 13 Changes in the R^2 values of the reflectance simulated by the Ross-Li model with NDVI for 5 cover types. In the calculation of R^2, simulated and observed reflectance is binned at 0.1 interval of NDVI

4 CONCLUSIONS

The ability of the Ross-Li model in conjunction with the MCD43A1 data to simulate bidirectional reflectance in the NIR band is assessed using globally distributed POLDER-3 BRDF data selected from the global POLDER-3/PARASOL BRDF archive. The following conclusions can be drawn.

(1) Overall, the Ross-Li model is able to simulate the bidirectional reflectance of ground objects efficiently. The R^2 and RMSE of simulated reflectance are 0.934 and 0.016, respectively. Forests have the largest RMSE of simulated reflectance, followed by shrubs, croplands, grasslands, and barren lands. On average, simulated reflectance is 5.2% lower than the POLDER-3 data.

(2) The Ross-Li model does not adequately account for the hotspot effects. It underestimates the hotspot reflectance by 14%,

with R^2 equal to 0.824 and RMSE equal to 0.07. The errors in simulated hotspot reflectance depend on land cover types. The coniferous forests have the largest underestimation (18.6%) of hotspot reflectance simulated by the Ross-Li model (RMSE equals 0.083), followed by broadleaved forests with the underestimation and RMSE of simulated hotspot reflectance equal to 16% and 0.076, grasslands and croplands with the underestimation of simulated reflectance equal to about 15% and RMSE equal to 0.07 and 0.068, shrubs and barren lands with the reflectance underestimated by 11% and 13%, respectively and RMSE values equal to 0.065 and 0.048.

(3) The reflectance simulated by the Ross-Li model is relatively accurate at nadir and darkspot directions. The departure of simulated reflectance from the POLDER-3 observations increases with the increases in solar zenith and view zenith angles.

(4) For grasslands and croplands, the accuracy of reflectance simulated by the Ross-Li model decreases with the increase in NDVI. However, for forests and shrubs, the discrepancy between reflectance simulated by the Ross-Li model and the POLDER-3 observations maximizes when NDVI approximately equals 0.5.

The hotspot reflectance is vital for the retrieval the structural parameters of vegetation canopy such as foliage clumping index. The modification to the volumetric kernel in the Ross-Li-M model improves the accuracy of simulated hotspot reflectance (R^2=0.839 and RMSE=0.043). However, underestimation of hotspot reflectance by the Ross-Li model is caused by both RossThick and LiSparseR kernels in it. Proper corrections for these two kernels are required to better the simulation of hotspot reflectance. Future efforts should be taken to address this issue.

Acknowledgements: The MODIS BRDF data are distributed by the Land Processes Distributed Active Archive Center (LP DAAC). The POLDER-3/PARASOL BRDFs databases have been elaborated by the LSCE, and provided by the POSTEL Service Centre. The POLDER-3/PARASOL data are from Centre National d'Etudes Spatiales (CNES).

REFERENCES

Bréon F M, Maignan F, Leroy M and Grant I. 2002. Analysis of the hot spot directional signatures measured from space. *Journal of Geophysical Research*, **107**(16): 4282–4296 DOI: 10.1029/2001JD001094

Chen J M, Menges C H and Leblanc S G. 2005. Global mapping of foliage clumping index using multi-angular satellite data. *Remote Sensing of Environment*, **97**(4): 447–457 DOI: 10.1016/j.rse.2005.05.003

Chen J M and Cihlar J. 1997. A hotspot function in a simple bidirectional reflectance model for satellite applications. *Journal of Geophysical Research*, **102**(D22): 25907–25913 DOI: 10.1029/97JD02010

Chen J M and Leblanc S G. 1997. A four-scale bidirectional reflectance model based on canopy architecture. *IEEE Transactions on Geoscience and Remote Sensing*, **35**(5): 1316–1337 DOI: 10.1109/36.628798

Chen Y M, Wang J D, Liang S L, Wang D W and Ma B. 2009. Comparison of MISR and MODIS bidirectional reflectance products. *Journal of Remote Sensing*, **13**(5): 808–815

Gao F, Schaaf C B, Strahler A H, Jin Y and Li X. 2003. Detecting vegetation structure using a kernel-based BRDF model. *Remote Sensing of Environment*, **86**(2): 198–205 DOI: 10.1016/S0034-4257(03)00100-7

Hautecoeur O and Leroy M. 2000. An accuracy assessment experiment of the BRDF measured at coarse spatial resolution from space. *International Journal of Remote Sensing*, **21**(15): 2957–2963 DOI: 10.1080/01431160050121375

Hu B X, Lucht W, Li X W and Strahler A H. 1997. Validation of kernel-driven semiempirical models for the surface bidirectional reflectance distribution function of land surfaces. *Remote Sensing of Environment*, **62**(3): 201–214 DOI: 10.1016/S0034-4257-(97)00082-5

Jiao Z T. 2008. The use of MODIS BRDF/Albedo Products to recover Land Surface Properties. Beijing: Dissertation of Beijing Normal University: 4–10

Jiao Z T, Wang J D, Xie L O, Zhang H, Yan G J, He L M and Li X W. 2005. Initial validation of MODIS albedo product by using field measurements and airborne multiangular remote sensing observations. *Journal of Remote Sensing*, **9**(1): 64–72

Leroy M and Roujean J L. 1994. Sun and view angle corrections on reflectances derived from NOAA/AVHRR data. *IEEE Transactions on Geoscience and Remote Sensing*, **32**(3): 684–697 DOI: 10.1109/36.297985

Li X W and Wan Z M. 1998. Comments on reciprocity in the BRDF modeling. *Progress in Natural Science in China*, **8**(3): 354–358

Li X W and Strahler A H. 1985. Geometric-optical modelling of a conifer forest canopy. *IEEE Transactions on Geoscience and Remote Sensing*, **23**(5): 705–721 DOI: 10.1109/TGRS.1985.289389

Li X W and Strahler A H. 1986. Geometric-optical bidirectional reflectance modelling of a conifer forest canopy. *IEEE Transactions on Geoscience and Remote Sensing*, **24**(6): 906–919 DOI: 10.1109/TGRS.1986.289706

Liang S L. 2004. Quantitative Remote Sensing of Land Surface. New York: Wiley

Liang S L, Fang H L, Chen M Z, Shuey C J, Walthall C, Daughtry C, Morisette J, Schaaf C B and Strahler A H. 2002. Validating MODIS land surface reflectance and albedo products: methods and preliminary results. *Remote Sensing of Environment*, **83**(1-2): 149–162 DOI: 10.1016/S0034-4257(02)00092-5

Liu J C, Schaaf C, Strahler A, Jiao Z T, Shuai Y M, Zhang Q L, Roman M, Augustine J A and Dutton E G. 2009. Validation of moderate resolution imaging spectroradiometer (MODIS) albedo retrieval algorithm: Dependence of albedo on solar zenith angle. *Journal of Geophysical Research*, **114**: D01106. DOI: 10.1029/2008JD009969

Lucht W, Schaaf C B and Strahler A H. 2000. An algorithm for the retrieval of albedo from space using semiempirical BRDF models. *IEEE Transactions on Geoscience and Remote Sensing*, **38**(2): 977–998 DOI: 10.1109/36.841980

Maignan F, Bréon F M and Lacaze R. 2004. Bidirectional reflectance of Earth targets: Evaluation of analytical models using a large set of spaceborne measurements with emphasis on the hot spot. *Remote Sensing of Environment*, **90**(2): 210–220 DOI: 10.1016/j.rse.2003.12.006

Nicodemus F E, Richmond J C, Hsia J J, Ginsberg I W and Limperis

T. 1977. Geometrical Considerations and Nomenclature for Reflectance. NBS Monograph 160. Washington, D.C.: National Bureau of Standards, U.S. Department of Commerce:

Ross J. 1981. The radiation regime and architecture of plant stands. Hague: Dr. W. Junk Publishers:

Roujean J L, Leroy M and Deschamps P Y. 1992. A bi-directional reflectance model of the Earth's surface for the correction of remote sensing data. *Journal of Geophysical Research*, **97**(D18): 20455–20468 DOI: 10.1029/92JD01411

Sandmeier S R and Deering D W. 1999. Structure analysis and classification of boreal forest using airborne hyperspectral BRDF data from ASAS. *Remote Sensing of Environment*, **69**(3): 281–295 DOI: 10.1016/S0034-4257(99)00032-2

Schaaf C B, Gao F, Strahler A H, Lucht W, Li X W, Tsang T, Strugnell N C, Zhang X Y, Jin Y F, Muller J P, Lewis P, Barnsley M, Hobson P, Disney M, Roberts G, Dunderdale M, Doll C, d'Entremont R, Hu B X, Liang S L, Privette J L and Roy D P. 2002. First operational BRDF, albedo and nadir reflectance products from MODIS. *Remote Sensing of Environment*, **83**(1-2): 135–148 DOI: 10.1016/S0034-4257(02)00091-3

Wanner W, Li X and Strahler A H. 1995. On the derivation of kernels for kernel-driven of bidirectional reflectance. *Journal of Geophysical Research*, D**100**: 21077–21089 DOI: 10.1029/95JD02371

Wanner W, Strahler A H, Hu B, Lewis P, Muller J P, Li X, Schaaf C L B and Barnsley M J. 1997. Global retrieval of bidirectional reflectance and albedo over land from EOS MODIS and MISR data: Theory and algorithm. *Journal of Geophysical Research*, **102**(17): 143–161 DOI: 10.1029/96JD03295

Wu A, Li Z and Cilhar J. 1995. Effects of land cover type and greenness on advanced very high resolution radiometer bidirectional reflectances: Analysis and removal. *Journal of Geophysical Research*, **100**(D5): 9179–9192 DOI: 10.1029/95JD00512

Xu X R. 2005. Remote Sensing Physics. Beijing: Peking University Press: 4

Yang H, Li X W and Gao F. 2002. An algorithm for the retrieval of albedo from space using new GO kernel-driven BRDF model. *Journal of Remote Sensing*, **6**(4): 246–251

利用POLDER数据验证MODIS BRDF模型参数产品及Ross-Li模型

朱高龙[1,2]，居为民[1]，陈镜明[1,3]，柳艺博[1]，朱敬芳[1]，邢白灵[1]

1. 南京大学 国际地球系统科学研究所，江苏 南京 210093；
2. 闽江学院 地理科学系，福建 福州 350108；
3. *Department of Geography, University of Toronto, Toronto, Ontario, M5S 3G3, Canada*

摘　要：将MODIS BRDF模型参数产品(MCD43A1)模拟的近红外波段反射率与从POLDER-3/PARASOL BRDF全球数据集中筛选的9961个像元的BRDF观测数据进行对比，验证了MCD43A1所采用的RossThick-LiSparseR BRDF 模型(Ross-Li模型)拟合二向反射的能力。结果表明，Ross-Li模型总体上可以有效地模拟地物的二向反射，所有像元的近红外波段反射率模拟值与POLDER-3观测数据之间的R^2达到0.943，RMSE为0.016，模拟反射率比POLDER-3数据总体偏低5.2%。但Ross-Li模型明显低估了热点反射率，热点模拟结果比POLDER-3数据平均偏低14%，模拟值的R^2为0.824，RMSE为0.07。热点反射率模拟误差与地表覆盖类型有关，针叶林热点反射率模拟值偏低最严重，其次是阔叶林、草地与农田，灌木与裸地热点反射率模拟值偏低相对较小。通过修正Ross-Li模型中的体散射核，可以明显改善热点反射率的模拟效果($R^2 = 0.839$，RMSE = 0.043)。Ross-Li模型对天底、暗点等特征方向反射率的模拟较为准确。Ross-Li模型的模拟精度随太阳天顶角和观测天顶角的增大而降低。对于农田与草地而言，Ross-Li模型的模拟精度随NDVI的增加而降低；但在森林与灌木覆盖条件下，当NDVI约为0.5时，Ross-Li模型的模拟效果最差。

关键词：MODIS，POLDER，热点反射率，Ross-Li模型，BRDF模型参数产品

中图分类号：TP702　　　**文献标志码**：A

引用格式：朱高龙，居为民，陈镜明，柳艺博，朱敬芳，邢白灵．2011．利用POLDER数据验证MODIS BRDF模型参数产品及Ross–Li模型．遥感学报，**15**(5): 875–894
Zhu G L, Ju W M, Chen J M, Liu Y B, Zhu J F and Xing B L. 2011. Validation of MODIS BRDF model parameters product and the Ross-Li model with POLDER data. *Journal of Remote Sensing*, **15**(5): 875–894

1　引　言

双向反射率分布函数(Bidirectional Reflectance Distribution Function, BRDF)描述了地表反射率随太阳和观测角度变化的各项异性特征(Nicodemus 等，1977)，它提供的地物方向谱信息有助于提取地表目标结构参数。随着具有多角度观测能力的传感器，如POLDER (Polarization and Directionality of Earth Reflectance) 和MISR (Multiangle Imaging Spectroradiometer) 等日益增多，BRDF在定量遥感中的应用得到越来越广泛的重视，如用于获取地表反照率(Wanner 等，1997；Schaaf 等，2002)、多时相分析对不同时相遥感角度的规一化处理(Leroy 和 Roujean，1994；Wu 等，1995)，以及利用特征方向谱(如热点、暗点、天底、主平面和主垂面等)或者BRDF模型参数构造各种指数，用于植被分类、叶面积指数(LAI)和叶片聚集度系数等植被结构参数反演(Sandmeier 和 Deering，1999；Gao 等，2003；Chen 等，2005)。

POLDER和MISR是目前可以在全球进行BRDF观

收稿日期：2010-07-11；**修订日期**：2010-11-16

基金项目：国家高技术研究发展计划项目(863计划)(编号：2009AA12Z134); 国家自然科学基金项目(编号：40871240/D011004)；遥感科学国家重点实验室开放基金资助(编号：2009KFJJ014)

第一作者简介：朱高龙(1974—　)，男，副教授，主要从事多角度光学植被遥感研究。E-mail: zhugaolong@163.com。

通信作者简介：居为民(1963—　)，男，教授，博士生导师，主要从事生态环境遥感和全球变化研究。E-mail: juweimin@nju.edu.cn。

测的传感器，但是POLDER数据的空间分辨率约为6 km，难以满足全球变化研究的需求；尽管MISR数据的空间分辨率较高(275 m—1.1 km)，但由于轨道幅宽较窄，难以观测到热点和暗点的反射。采用半经验的核驱动模型(Roujean 等，1992；Wanner 等，1995；Lucht 等，2000)对16天累积的MODIS (Moderate resolution Imaging Spectroradiometer) 观测数据进行拟合生成的MODIS BRDF模型参数产品，为研究地物反射各向异性行为提供了新途径。但是MODIS BRDF模型参数产品存在着低估热点反射率的现象(Chen和Cihlar，1997；Bréon 等，2002；Maignan 等，2004)。前人开展了大量的验证MODIS BRDF及反照率产品的研究工作(Hu 等，1997；Liang 等，2002；焦子锑 等，2005；Liu 等，2009)。在大量有代表性的地点进行实地观测是评价BRDF产品质量的常用手段，但野外测量成本较高，而且大多只能获取点上的数据，覆盖范围小，难以直接检验中等分辨率的MODIS BRDF模型参数产品。

不同星载或机载传感器获取的同类产品之间的对比为验证BRDF产品提供了一种有效的方法(Hautecoeur和Leroy，2000)。陈永梅等(2009)通过将MISR和MODIS反射率产品与根据它们的BRDF模型参数产品计算的反射率进行交叉验证，分析了这两种BRDF模型参数产品的二向反射外推能力。但是由于MISR难以观测到主平面上的地物反射特性，所以无法验证MODIS BRDF模型参数产品模拟热点等特征方向反射率的精度。而热点与暗点包含叶片聚集度指数和LAI等冠层结构参数的重要信息，所以有必要对MODIS BRDF模型参数产品和Ross-Li模型外推热点与暗点反射率的能力进行验证与评价。本文根据POLDER传感器易于观测热点和暗点反射的特点，利用全球分布的POLDER BRDF数据验证MODIS BRDF模型参数产品外推不同角度反射率的能力，并分析MODIS BRDF模型参数产品的二向反射外推误差与地表覆盖类型和植被密度之间的关系。

2　数据与方法

2.1　POLDER-3 BRDF产品

搭载在PARASOL卫星上的POLDER-3采用旋转式的CCD面阵成像，几乎每天覆盖全球1次，星下点分辨率为6 km × 7 km，最大视场角为114º；由于地球曲率影响，沿轨道方向的观测天顶角可达到 ± 61º，垂直于轨道方向观测天顶角可达到 ± 50º。POLDER-3利用视场重叠获取多角度数据，单次过境时每个像元最多可有16个不同角度的观测。由于每次过境轨道的偏移引起观测角度的变化，如果天气条件良好，经过连续多天的观测，基本可以实现全方位的观测。POLDER-3具有9个可见光与近红外波段，其中包含3个偏振波段。POLDER-3多角度观测数据经过辐射校正、空间配准、去云、大气校正等一系列处理，得到地表反射率数据，像元分辨率为6.17 km。法国气候与环境科学实验室(LSCE)选择其中质量最优的地表反射率数据，分别基于IGBP与GLC2000土地覆盖分类系统，生产了全年和分月的4个BRDF产品数据集。本研究使用的数据是基于GLC2000分类系统的分月BRDF产品数据集。为保证较高的像元均质性，该数据集要求在每个像元内的主要地表覆盖类型至少占该像元面积的80%以上。该数据集总共收集了2005年11月至2006年10月全球各种地表覆盖类型的20985个像元数据，每个像元按月累积各月内的观测数据并存储为一个ASCII文件，其数据项包括该像元的经纬度、GLC2000地表覆盖类型、NDVI、像元均质度、观测日期、太阳天顶角、观测天顶角、相对方位角以及各波段的地表反射率(图1)。单个像元一个月累积的观测角度最多可达到300多个，基本可以实现全方位的角度观测(图2)。

latitude	longitude	GLC2000_class	NDVI	nb_orbit	nb_dir	homogeneity(%)
25.69	99.71	4	0.45	6	84	85.71

yymmdd	thetaS	thetaV	RelAzi	R490	R565	R670	R765	R865	R1020
060201	44.97	58.67	37.06	0.062	0.090	0.104	0.225	0.266	0.325
060201	44.97	53.63	38.07	0.064	0.089	0.101	0.221	0.265	0.320
060201	44.97	47.62	39.47	0.063	0.088	0.101	0.214	0.256	0.312
060201	44.97	40.41	41.55	0.056	0.078	0.105	0.205	0.250	0.304
060201	44.97	31.86	45.04	0.048	0.070	0.088	0.190	0.229	0.280
060201	44.97	22.02	52.13	0.040	0.063	0.079	0.172	0.210	0.260
060201	44.97	11.92	72.89	0.040	0.060	0.080	0.158	0.191	0.243
060201	44.97	8.48	145.03	0.036	0.055	0.071	0.143	0.173	0.220
060201	44.97	17.16	185.79	0.031	0.049	0.059	0.128	0.157	0.199
060201	44.97	27.35	196.82	0.028	0.042	0.057	0.120	0.148	0.188
060201	44.97	36.53	201.53	0.028	0.041	0.054	0.115	0.143	0.179
060201	44.97	44.34	204.13	0.027	0.039	0.050	0.111	0.136	0.176
060201	44.97	50.88	205.78	0.028	0.039	0.047	0.106	0.133	0.169
060201	44.97	56.34	206.93	0.027	0.036	0.044	0.109	0.133	0.167
060203	43.59	60.70	52.07	0.051	0.073	0.086	0.191	0.232	0.282
060203	43.59	56.47	55.74	0.047	0.071	0.087	0.186	0.226	0.273

……

图1　ASCII 格式的POLDER-3 BRDF数据文件示例
(latitude：纬度/(º)，longitude：经度/(º)，GLC2000_class：覆盖类型，nb_orbit：过境轨道个数，nb_dir：观测方向个数，homogeneity：均质度/(%)，yymmdd：观测日期，thetaS：太阳天顶角/(º)，thetaV：观测天顶角/(º)，RelAzi：相对方位角/(º)，R490、R565、R670、R765、R865、R1020是各波长/(nm)地表反射率)

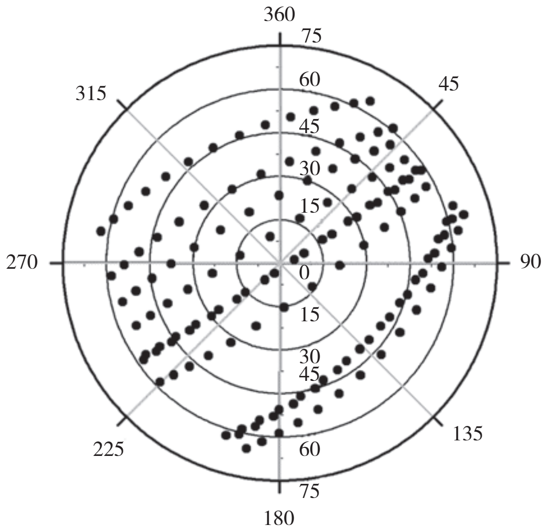

图2　POLDER-3像元观测角度分布示例(半径为观测天顶角/(°)，圆周为相对方位角/(°))

2.2　MODIS BRDF模型参数产品

本研究采用的MODIS BRDF模型参数产品(MCD43A1)是由16天连续观测的MODIS(Terra + Aqua)反射率数据拟合而成，每隔8天生成一期数据，像元的空间分辨率为463.3 m。MCD43A1是基于核驱动的RossThick-LiSparseR BRDF 模型(Ross-Li模型)生成的(Roujean 等，1992；Wanner 等，1995；Lucht 等，2000)。该模型用有一定物理意义的核的线性组合来拟合地表的二向性反射特征，目前005版本的核组合为RossThick核与LiSparseR核，其简化的表达式如下：

$$R(\theta,\vartheta,\varphi)=f_{iso}+f_{vol}K_{vol}(\theta,\vartheta,\varphi)+f_{geo}K_{geo}(\theta,\vartheta,\varphi) \quad (1)$$

$$K_{vol}(\theta,\vartheta,\varphi)=\frac{(\pi/2-\xi)\cos\xi+\sin\xi}{\cos\theta+\cos\vartheta}-\frac{\pi}{4} \quad (2)$$

$$K_{geo}(\theta,\vartheta,\varphi)=O(\theta,\vartheta,\varphi)-\sec\theta-\sec\vartheta+\frac{1}{2}(1+\cos\xi)\sec\theta\sec\vartheta \quad (3)$$

$$O(\theta,\vartheta,\varphi)=\frac{1}{\pi}(t-\sin t\cos t)(\sec\theta+\sec\vartheta) \quad (4)$$

$$\cos t=2\frac{\sqrt{D^2+(\tan\theta\tan\vartheta\sin\phi)^2}}{\sec\theta+\sec\vartheta} \quad (5)$$

$$D=\sqrt{\tan^2\theta+\tan^2\vartheta-2\tan\theta\tan\vartheta\cos\varphi} \quad (6)$$

$$\cos\xi=\cos\theta\cos\vartheta+\sin\theta\sin\vartheta\cos\varphi \quad (7)$$

式中，$R(\theta,\vartheta,\varphi)$ 是二向反射率，θ为入射天顶角，ϑ为观测天顶角，φ为太阳与观测的相对方位角；$K_{vol}(\theta,\vartheta,\varphi)$和$K_{geo}(\theta,\vartheta,\varphi)$分别为体散射核和几何光学散射核，它们都是入射角和观测角的函数。f_{iso}、f_{vol}和f_{geo}为各个核的系数，分别表示各向同性散射、体散射、几何光学散射所占的权重。ξ是散射角，即太阳入射光与观测视线的夹角。该模型算法根据16天周期内不同角度观测的反射率$R(\theta,\vartheta,\varphi)$，以及根据式(1)，式(2)计算的$K_{vol}(\theta,\vartheta,\varphi)$和$K_{geo}(\theta,\vartheta,\varphi)$，利用最小二乘法拟合观测数据确定$f_{iso}$、$f_{vol}$和$f_{geo}$，并作为MODIS BRDF模型参数产品提供给用户使用。用户利用这3个模型参数，根据上述方程就可以求出任意入射角和观测角条件下的二向反射。

2.3　数据准备与处理

为验证MODIS BRDF模型参数产品的二向反射外推能力，从LP DAAC (Land Processes Distributed Active Archive Center)下载了与POLDER-3 BRDF数据获取时间对应、且每景包含较多POLDER-3 BRDF像元的1193景MCD43A1数据和相应的质量文件MCD43A2。这些数据基本涵盖了全球范围的主要地表覆盖类型、各种等级的植被覆盖度，时间跨度为2005年11月至2006年10月。因为提取叶片聚集度系数常用近红外波段的热点和暗点反射率，本研究仅验证近红外波段MODIS BRDF模型参数产品的模拟二向反射精度。MODIS 近红外波的段波长范围为841 nm—876 nm，POLDER-3近红外波段中心波长为865 nm，谱宽为40 nm，两种传感器的近红外波段设置基本相同，具有可比性。

2.3.1　像元空间匹配

POLDER-3 BRDF产品与MODIS BRDF模型参数产品都采用正弦等积投影，POLDER-3 BRDF产品把全球分为3240 × 6480个像元。MODIS BRDF模型参数产品把全球分为18 × 36景，每景包含2400 × 2400个像元。一个POLDER-3 BRDF像元相当于13 × 13个MODIS BRDF模型参数像元。利用式(8)—(11)可以准确获取POLDER-3像元对应的MODIS像元的起始行列数。

$$V=\mathrm{INT}((lin-1)/180) \quad (8)$$

$$H=\mathrm{INT}((col-1)/180) \quad (9)$$

$$r=\mathrm{INT}(40/3\times\mathrm{MOD}((lin-1),180)) \quad (10)$$

$$p=\mathrm{INT}(40/3\times\mathrm{MOD}((col-1),180)) \quad (11)$$

式中，lin、col为POLDER-3像元的行列数，V、H为MODIS像元所在景的编号(V，H)，r、p为对应

MODIS像元在该景中的起始行列数(即对应的13×13个MODIS像元左上角像元的行列数)，INT为求整运算，MOD为求模运算。

2.3.2 数据处理方法

首先根据每一个POLDER-3 BRDF像元的行列数，利用式(8)—(11)确定与其对应的13×13个MODIS BRDF模型参数像元所在的景号及起始行列数。由于POLDER-3每个像元的BRDF数据是按月累积的观测数据，而MODIS BRDF模型参数产品是采用16天累积的MODIS观测数据进行拟合生成的。因此需要根据每个POLDER-3像元观测数据的获取时间找出同期的近红外波段的MODIS BRDF模型参数产品，再从MCD43A2中提取相应的近红外波段BRDF产品的质量信息。如果其质量等级都为0(best quality, full inversion)或1(good quality, full inversion)，则将MODIS BRDF模型参数代入式(1)，根据同期的POLDER-3 BRDF数据中提供的太阳天顶角、观测天顶角和相对方位角信息，计算每个MODIS像元的近红外波段反射率，将计算的169个MODIS像元的反射率算术平均值与POLDER-3观测的近红外波段反射率进行比较，进而评价MODIS BRDF模型参数产品的二向反射外推能力。虽然POLDER-3与MODIS像元空间尺度悬殊，但所选像元均质度都大于80%，根据Liang(2004)的研究结果表明BRDF升尺度是线性的，因此，可以不考虑空间尺度效应的影响。

3 结果与分析

3.1 数据处理结果

由于Ross-Li模型不适用于冰雪等地表覆盖类型，为排除非植被像元可能带来的评价结果误差，本文以NDVI大于0.15为标准，共选择了9961个有效POLDER-3 BRDF像元验证MODIS BRDF模型参数产品的二向反射外推能力，这些像元包括了19种GLC2000地表覆盖类型(表1)，对水体、冰雪、居民地3类像元不作考虑。每种地表类型覆盖类型的像元个数如表1所示。单个像元最多的观测角度为199个，最少的观测角度为6个，所有像元的观测角度总数为714652个，平均每个像元在其对应的MODIS BRDF数据的16天周期中有72个不同角度的观测。这些像元NDVI的变化范围从0.15—0.87，每种地表覆盖类型的NDVI值都有较大的变化区间。太阳天顶角θ的变化范围从11.4º到74.7º，观测天顶角ϑ的变化范围从0.1º到67.6º，相对方位角φ的变化范围从0º到360º。

表1 POLDER-3 BRDF 数据处理结果统计信息

GLC2000地表覆盖类型	POLDER像元数	观测次数Nobs	NDVI范围	NDVI平均值	太阳天顶角范围/(º)	POLDER平均反射率	Ross-Li模型模拟值	模拟值的RMSE
常绿阔叶林	455	30370	0.29—0.84	0.71	15.4—66.2	0.256	0.251	0.020
郁闭的落叶阔叶林	1002	78400	0.18—0.87	0.55	11.4—70.3	0.235	0.232	0.016
稀疏的落叶阔叶林	378	30110	0.20—0.79	0.43	17.4—62.3	0.213	0.209	0.014
常绿针叶林	545	39452	0.17—0.86	0.51	12.0—74.7	0.202	0.208	0.017
落叶针叶林	628	35762	0.15—0.81	0.56	28.6—72.8	0.221	0.215	0.018
不同类型的树木	569	35684	0.25—0.87	0.55	13.7—74.5	0.222	0.217	0.017
被淡水淹的树木	13	709	0.60—0.80	0.66	26.3—48.2	0.249	0.240	0.022
被咸水淹的树木	58	4136	0.15—0.73	0.51	15.3—52.1	0.239	0.236	0.020
树木和其他类型混合	720	41858	0.21—0.86	0.63	12.2—74.4	0.240	0.238	0.017
燃烧过的树木	436	24405	0.24—0.81	0.55	28.3—74.7	0.216	0.212	0.017
常绿灌木	802	52483	0.15—0.87	0.63	12.2—74.5	0.269	0.267	0.017
落叶灌木	563	49367	0.15—0.73	0.32	11.5—74.6	0.224	0.221	0.013
不同密度的草本	732	60783	0.15—0.83	0.30	14.8—73.4	0.249	0.247	0.014
稀疏的草本或灌木	725	60016	0.15—0.64	0.27	15.7—72.6	0.251	0.248	0.013
被淹的灌木和草本	568	39177	0.15—0.82	0.57	16.7—73.8	0.259	0.256	0.019
耕作与管理区	700	59156	0.15—0.85	0.38	12.6—71.7	0.261	0.257	0.014
农田与树木混合	453	27481	0.17—0.87	0.69	15.9—62.0	0.293	0.293	0.017
农田和灌木混合	535	39580	0.15—0.79	0.41	14.7—73.6	0.272	0.270	0.015
裸地	79	5723	0.15—0.44	0.21	19.8—68.0	0.218	0.218	0.012
所有类型	9961	714652	0.15—0.87	0.50	11.4—74.7	0.244	0.241	0.016

图3是Ross-Li模型模拟的所有观测角度的近红外反射率与POLDER-3观测数据的比较结果。可以看出，Ross-Li模型总体上成功地模拟了地物的二向反射，模拟的714652个不同观测角度反射率的R^2达到0.943，RMSE为0.016，模拟反射率的RMSE表现为森林最大，其次为灌木、农田、草地和裸地，反射率的模拟值相对于POLDER-3观测数据总体偏低5.2%。图4是图1文件中像元主平面(0°≤ φ≤ 10°或170°≤ φ≤190° 或350°≤φ≤360°)上Ross-Li模型模拟的近红外反射率与POLDER-3观测值的对比，可以看出Ross-Li模型严重地低估了热点反射率，而其他角度的反射率模拟值与POLDER-3观测值较为接近。

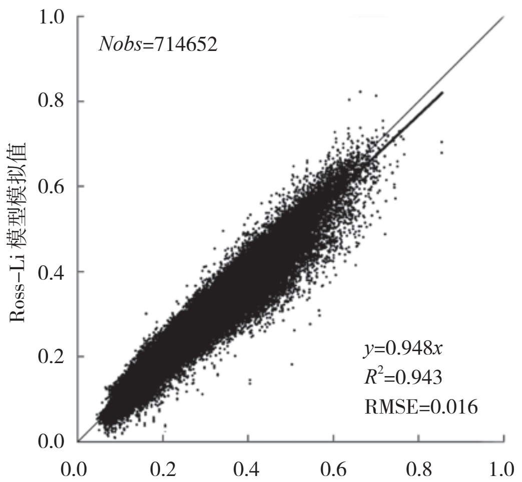

图3 Ross-Li模型模拟的所有观测角度反射率与POLDER-3观测值比较

3.2 Ross–Li模型对热点反射率模拟精度评价及其订正

当传感器视线与入射光线完全重合时，传感器视域内都是光照面，看不到阴影面，此时传感器观测到很强的反射峰，即热点现象；当视线逐渐偏移入射光线时，传感器视域内阴影面积逐渐增大，观测到的反射率迅速下降(图4)。Ross-Li模型低估热点反射率是由该模型的假设条件导致的：RossThick核(体散射核)是由Ross提出的适合于水平均一连续致密植被的辐射传输模型推导出来的(Ross，1981；Roujean 等，1992)，它没有考虑植被叶片相互遮阴的情况；LiSparseR核(几何光学散射核)是从Li-Strahler几何光学模型(Li 和 Strahler，1985，1986；焦子锑，2008)推导出来的，适合于描述稀疏植被冠层(Wanner 等，1997；Lucht 等，2000)，但它把树冠简化为不透光的球体或椭球体，其本质是单次散射模型(徐希孺，2005)，虽然考虑太阳直射光辐照下的光照面与阴影面(4分量)的差别，但没有考虑树冠内部叶片随入射与观测角度变化产生的遮阴现象。虽然LiSparseR核在热点位置有一个小的反射峰(Lucht 等, 2000)，但它尚不能捕捉到完全的热点信号。因此Ross-Li模型没有完全考虑热点现象。

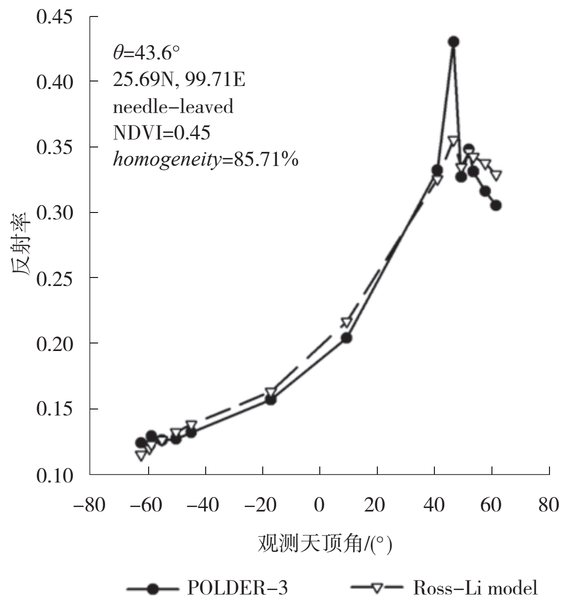

图4 针叶林像元主平面Ross-Li模型模拟值与POLDER-3观测值对比(横坐标正值为后向反射，负值为前向反射)

Chen和Cihlar(1997)基于4尺度几何光学模型(Chen和Leblanc，1997)，引入热点强度与宽度两个订正系数，修正了核驱动模型的几何光学核与体散射核，有效地改进了核驱动模型对热点反射的模拟效果。Maignan 等(2004)发展了一种简单的订正热点反射的方法，即保持几何光学散射核不变，仅对体散射核进行订正：

$$K_{vol}(\theta,\vartheta,\varphi)=\frac{(\pi/2-\xi)\cos\xi+\sin\xi}{\cos\theta+\cos\vartheta}(1+(1+\xi/\xi_0)^{-1})-\frac{\pi}{4} \tag{12}$$

式中，ξ为散射角，由式(7)给出；ξ_0是由散射体大小与冠层垂直密度比值决定的特征角度，一般取

1.5º。本研究利用上述Maignan方法(以下简称为Ross-Li-M 模型)对模拟的热点反射率进行订正。

以$0° \leq \varphi \leq 10°$ 或$350° \leq \varphi \leq 360°$ 并且$|\theta-\vartheta| \leq 2°$为条件，从所有观测角度数据集中筛选出5061个热点观测数据，用Ross-Li模型和Ross-Li-M模型分别模拟不同地表覆盖类型的近红外波段反射率，以模拟值为y，POLDER-3观测数据为x，进行回归分析($y=ax$)，结果如表2所示。Ross-Li模型模拟结果的回归系数**a**值的变化范围为0.806到0.916，R^2为0.569到0.913，RMSE为0.044到0.090。Ross-Li模型对热点反射率模拟的误差与地表覆盖类型有关。模拟的针叶林热点反射率偏低最严重(18.6%)，R^2最小(0.611)，RMSE最大(0.083)；阔叶林热点反射率偏低16%，R^2为0.8，RMSE为0.076；草地与农田热点反射率低估15%左右，R^2分别为0.803和0.843，RMSE分别为0.07和0.068；灌木与裸地热点反射率分别偏低11%和13%，R^2分别为0.868和0.803，RMSE分别为0.065和0.048。Ross-Li模型对针叶林热点反射率低估最严重，这是因为针叶林的冠层几何结构最为明显，叶片空间分布最不均匀，存在着最明显的热点现象；而农田与草地的冠层叶片分布相对比较均匀，热点现象不如针叶林显著，所以Ross-Li模型对这两种地表覆盖类型热点反射率的低估相对较小。从表2可以看出，除了“被淹的灌木和草本植被”类型外，Ross-Li-M 模型明显地改进了对热点反射率的模拟效果，消除了模拟的热点反射率系统性偏低的现象。

图5和图6显示两种模型模拟的5061个热点反射率与POLDER-3数据之间的对比。相对于原始的Ross-Li模型而言，改进后的Ross-Li-M模型的回归斜率从0.859变为1.028，R^2从0.824提高到0.839，RMSE从0.07降低到0.043，Ross-Li-M模型对反射率较大的热点模拟改进尤为明显。对于全部的714652个角度观测的模拟结果而言(图3和图7)，Ross-Li-M模型比Ross-Li模拟也有较大的改进，R^2从0.943提高到0.967，RMSE从0.016降低到0.015，模拟的反射率与POLDER-3数据之间的回归斜率由0.948变为1.027。

表2　Ross-Li模型和Ross-Li-M模型模拟的热点反射率与POLDER-3观测数据的比较

GLC2000地表覆盖类型	POLDER 热点观测数 *Nobs*	平均 NDVI	Ross-Li模型			Ross-Li-M模型		
			回归方程	R^2	RMSE	回归方程	R^2	RMSE
常绿阔叶林	243	0.72	y=0.859x	0.824	0.090	y=1.028x	0.839	0.044
郁闭的落叶阔叶林	558	0.54	y=0.852x	0.742	0.072	y=1.017x	0.814	0.036
稀疏的落叶阔叶林	211	0.43	y=0.815x	0.689	0.071	y=1.009x	0.840	0.027
常绿针叶林	285	0.54	y=0.820x	0.638	0.081	y=0.983x	0.800	0.034
落叶针叶林	244	0.60	y=0.806x	0.569	0.085	y=0.971x	0.795	0.037
不同类型的树木	237	0.55	y=0.840x	0.606	0.077	y=0.993x	0.811	0.033
被淡水淹的树木	8	0.68	y=0.855x	0.913	0.063	y=1.020x	0.797	0.031
被咸水淹的树木	14	0.45	y=0.908x	0.886	0.044	y=1.037x	0.818	0.041
树木和其他类型的混合	317	0.64	y=0.888x	0.859	0.068	y=1.020x	0.897	0.041
燃烧过的树木	209	0.52	y=0.827x	0.634	0.069	y=0.978x	0.822	0.028
常绿灌木	379	0.60	y=0.916x	0.828	0.065	y=1.047x	0.856	0.054
落叶灌木	307	0.33	y=0.844x	0.834	0.064	y=1.045x	0.847	0.038
不同密度的草本	416	0.30	y=0.847x	0.803	0.070	y=1.034x	0.778	0.043
稀疏的草本或灌木	487	0.27	y=0.857x	0.799	0.062	y=1.046x	0.804	0.038
被淹的灌木和草本植被	257	0.58	y=0.881x	0.740	0.061	y=1.124x	0.553	0.083
耕作与管理区	398	0.39	y=0.852x	0.843	0.068	y=1.041x	0.864	0.037
农田与树木混合	204	0.66	y=0.908x	0.817	0.064	y=1.041x	0.876	0.043
农田和灌木混合	247	0.40	y=0.853x	0.862	0.067	y=1.064x	0.882	0.043
裸地	40	0.21	y=0.873x	0.803	0.048	y=1.056x	0.891	0.028
所有类型	5061	0.48	y=0.859x	0.824	0.070	y=1.028x	0.839	0.043

注：x为POLDER-3观测的近红外波段地表反射率，y为Ross-Li模型或Ross-Li-M模型的模拟值

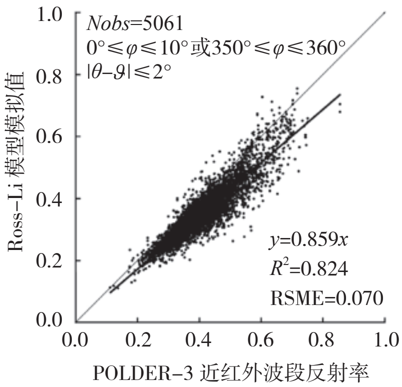

图5 Ross-Li模型模拟的热点反射率与POLDER-3数据的比较

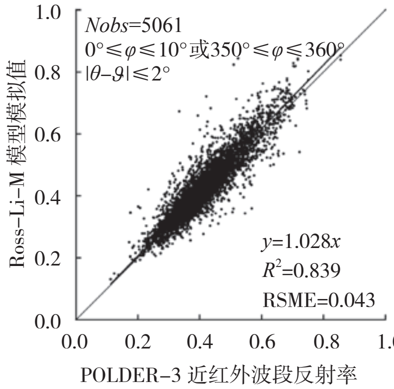

图6 Ross-Li-M模型模拟的热点反射率与POLDER-3数据的比较

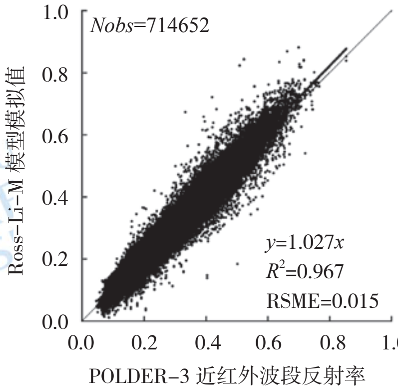

图7 Ross-Li-M模型模拟的所有观测角度反射率与POLDER-3数据的比较

3.3 Ross-Li模型外推能力随太阳天顶角与观测天顶角的变化

由于Ross-Li模型在热点处误差较大，为了评估Ross-Li模型外推能力随太阳天顶角与观测天顶角的变化，本研究从所有观测数据中剔除热点的观测数据，得到709591个不同角度的观测与模拟反射率数据对，以太阳天顶角1°为步长，将所有观测角度分组，分别统计各组的Ross-Li模型模拟反射率与POLDER-3观测反射率的线性回归关系的R^2和RMSE，用于评价太阳天顶角变化对Ross-Li模型外推能力的影响。从图8可以看出随太阳天顶角的增大，模拟反射率的R^2总体呈下降趋势，而RMSE呈上升趋势，当太阳天顶角大于65°时，模拟反射率的RMSE大于0.02。用同样的方法分析了Ross-Li模型外推能力随观测天顶角的变化(图9)，可以发现随观测天顶角的增大，模拟反射率的R^2总体呈下降趋势，RMSE呈上升趋势，这与Chen等(2009)研究结果相同。当观测天顶角大于63°时，模拟反射率的RMSE大于0.02。比较图8与图9，可以看出太阳天顶角对Ross-Li模型模拟精度的影响大于观测天顶角的影响。

在大观测天顶角时，Ross-Li模型产生较大误差的原因在于LiSparseR核是基于互易原理改写的LiSparse核，LiSparse核假定视场中植被及其阴影的总面积远小于视场总面积，其比值近似正比于sec(ϑ)(杨华 等，2002)，在大观测顶角条件下，这种假设就失效了，所以此时该模型计算的反射率误差很大，甚至出现负值。LiSparseR核虽然能够部分改善这种

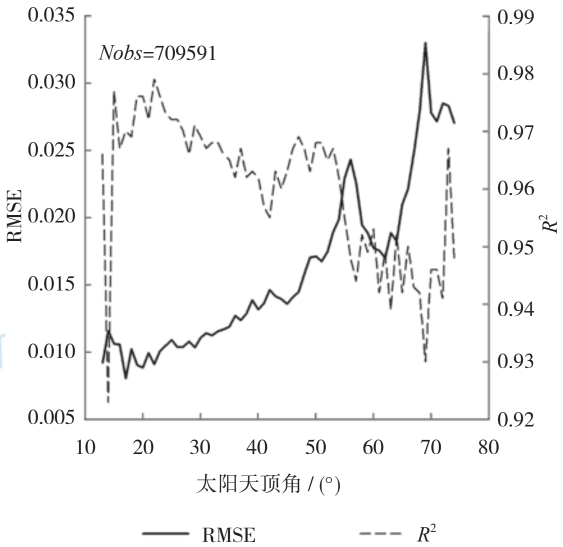

图8 Ross-Li模型外推能力随太阳天顶角的变化

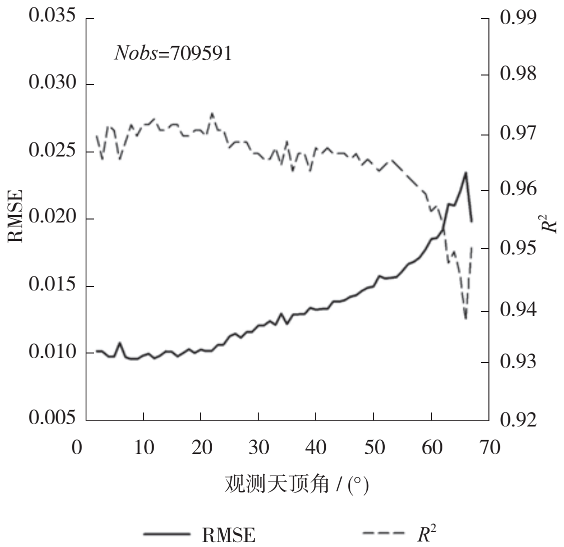

图9 Ross-Li模型外推能力随观测天顶角的变化

问题，但并不能完全消除大观测天顶角的影响。由于LiSparseR核是假定太阳入射角与传感器观测角可互易的核(Wanner 等，1995；Wanner 等，1997；Lucht 等，2000)，因此太阳天顶角变化的影响效果与观测天顶角变化的影响效果类似。虽然李小文和万正明(1998)认为以互易原理作为BRDF建模的先决条件缺乏依据，但本文暂不讨论该问题。

由于在植被分类或反演植被结构参数时，还经常利用天底或暗点等特征方向的反射率，因此有必要验证这些特征方向的BRDF模型模拟精度。本研究从所有POLDER-3观测角度中，根据$\vartheta \leqslant 10°$ 选择天顶观测数据，根据$45° \leqslant \vartheta \leqslant 50°$ 且$170° \leqslant \varphi \leqslant 190°$ 选择暗点观测数据，并与Ross-Li模型计算的反射率进行相关分析，可以发现Ross-Li模型对于天底和暗点反射的模拟精度比较好，R^2分别为0.968和0.947，RMSE分别为0.01和0.011(图10和11)。

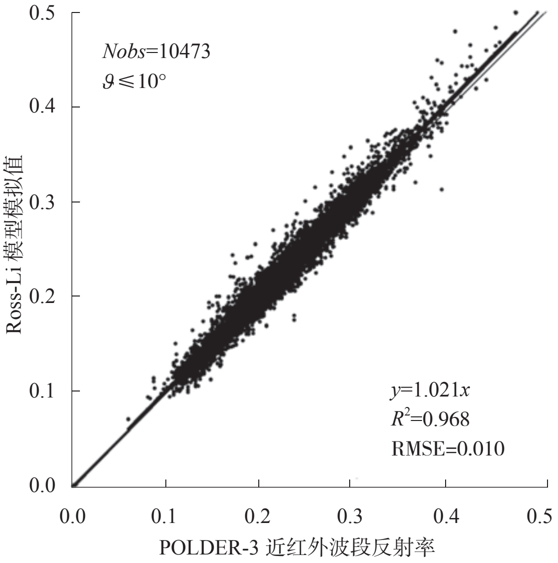

图10 Ross-Li模型模拟的天底反射率与POLDER-3数据比较

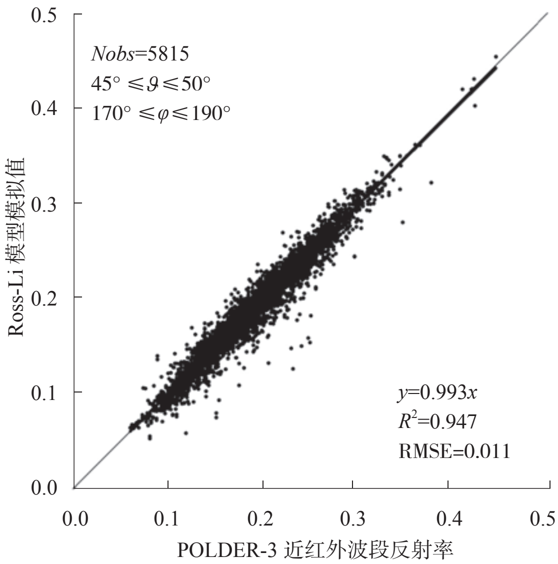

图11 Ross-Li模型模拟的暗点反射率与POLDER-3数据比较

3.4 Ross–Li模型外推能力随NDVI的变化

为了评价不同植被密度条件下Ross-Li模型的外推能力，本研究选择了落叶阔叶林、落叶针叶林、常绿灌木、草地和农田5种主要的地表覆盖类型，分析Ross-Li模型反射率模拟值与POLDER-3观测数据的一致性随NDVI的变化。对以上每一种植被类型，分别计算NDVI间隔为0.1的区间内的所有观测角度的反射率模拟值与POLDER-3观测值之间线性回归关系的R^2和RMSE。从图12和图13可以看出，随着NDVI的增加，Ross-Li模型模拟的农田与草地反射率的RMSE总体呈上升趋势，而R^2总体呈下降趋势。而对于落叶阔叶林、落叶针叶林与常绿灌木而言，植被密度中等时(NDVI约为0.5)，Ross-Li模型模拟的反射率的RMSE较大，R^2较小。可能的一个原因是森林与灌木冠层几何结构特征明显，在NDVI为中等时阴影效应最强(稀疏离散植被阴影重叠的概率较小)，热点现象显著，而Ross-Li模型没有充分考虑热点效应，因此此时模拟的反射率RMSE最大。

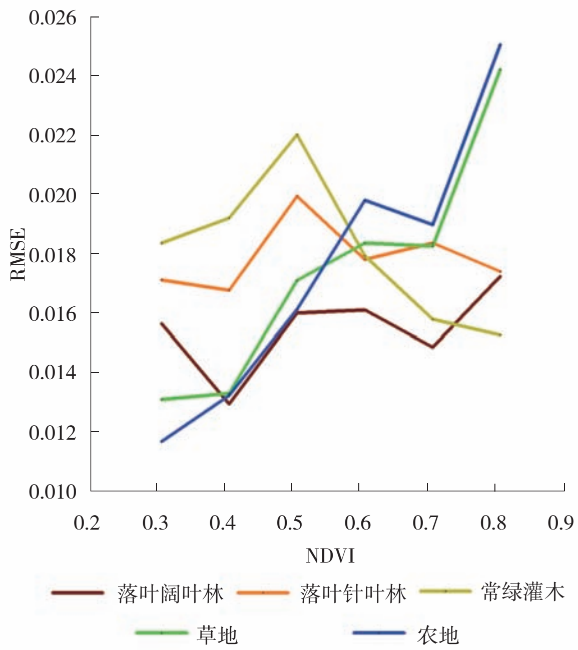

图12 Ross-Li模型模拟值与POLDER-3观测值的RMSE随NDVI的变化

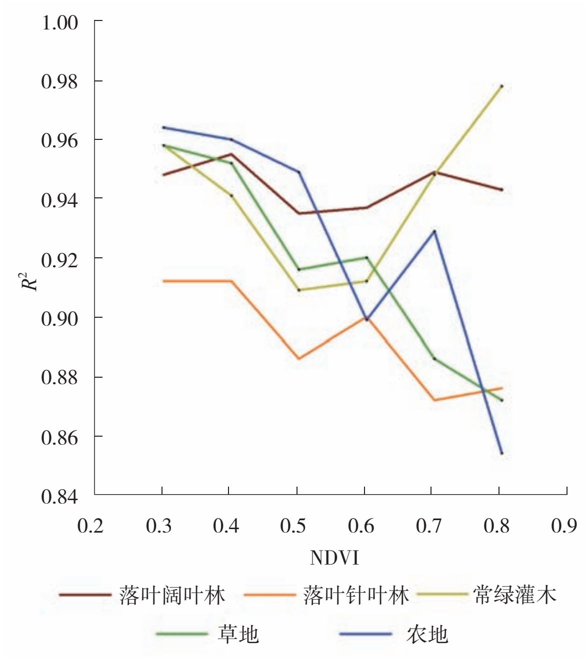

图13 Ross-Li模型模拟值与POLDER-3观测值的R^2随NDVI的变化

4 结论

本文利用全球分布的各种地表覆盖类型的POLDER-3/PARASOL BRDF数据验证MODIS BRDF模型参数产品和Ross-Li模型模拟近红外波段反射率的精度，结果表明：

(1)Ross-Li模型总体上成功地模拟了地物的二向反射，模拟值与实测值的R^2达到0.943，RMSE为0.016，模拟反射率的RMSE为森林>灌木>农地>草地>裸地，总体偏低5.2%。

(2)Ross-Li模型没有充分考虑热点效应，对于热点反射率模拟精度较差，R^2为0.824，RMSE为0.07，平均低估了14%。其中针叶林低估最明显(18.6%)，RMSE为0.083；阔叶林次之，低估16%，RMSE为0.076；草地与农地低估15%左右，RMSE分别为0.07和0.068；灌木与裸地低估11%和13%，RMSE分别为0.065和0.048。

(3)Ross-Li模型二向反射模拟精度随太阳天顶角和观测天顶增大而降低；Ross-Li模型对于天底、暗点等特征方向的模拟较为准确。

(4)Ross-Li模型对农田与草地反射率的模拟精度随NDVI的增加而降低，而对森林与灌木反射率的模拟在NDVI约为0.5时误差最大。

热点反射包含了冠层结构特征的重要信息，可用于冠层结构参数的反演。本文采用简单改写体散射核的Ross-Li-M模型改进了热点反射率的模拟效果(R^2 = 0.839，RMSE = 0.043)。但是Ross-Li模型对热点反射率的低估，是由体散射核与几何光学核共同造成的，为了更准确模拟热点反射率，需要同时订正体散射核与几何光学核，这是有待于进一步的研究。

志 谢 本文所用的MODIS BRDF数据由美国陆地过程分布式活动档案中心(LP DAAC)提供，POLDER-3/PARASOL BRDF数据由法国气候与环境科学实验室(LSCE)生产，并由POSTEL服务中心提供，POLDER-3/PARASOL数据来自国家空间研究中心。

REFERENCES

Bréon F M, Maignan F, Leroy M and Grant I. 2002. Analysis of the hot spot directional signatures measured from space. *Journal of Geophysical Research*, **107**(16): 4282–4296 DOI: 10.1029/2001JD001094

Chen J M, Menges C H and Leblanc S G. 2005. Global mapping of foliage clumping index using multi-angular satellite data. *Remote Sensing of Environment*, **97**(4): 447–457 DOI: 10.1016/j.rse.2005.05.003

Chen J M and Cihlar J. 1997. A hotspot function in a simple bidirectional reflectance model for satellite applications. *Journal of Geophysical Research*, **102**(D22): 25907–25913 DOI: 10.1029/97JD02010

Chen J M and Leblanc S G. 1997. A four-scale bidirectional reflectance model based on canopy architecture. *IEEE Transactions on Geoscience and Remote Sensing*, **35**(5): 1316–1337 DOI: 10.1109/36.628798

Chen Y M, Wang J D, Liang S L, Wang D W and Ma B. 2009. Comparison of MISR and MODIS bidirectional reflectance products. *Journal of Remote Sensing*, **13**(5): 808–815

Gao F, Schaaf C B, Strahler A H, Jin Y and Li X. 2003. Detecting vegetation structure using a kernel-based BRDF model. *Remote Sensing of Environment*, **86**(2): 198–205 DOI: 10.1016/S0034-4257(03)00100-7

Hautecoeur O and Leroy M. 2000. An accuracy assessment experiment of the BRDF measured at coarse spatial resolution from space. *International Journal of Remote Sensing*, **21**(15): 2957–2963 DOI: 10.1080/01431160050121375

Hu B X, Lucht W, Li X W and Strahler A H. 1997. Validation of kernel-driven semiempirical models for the surface bidirectional reflectance distribution function of land surfaces. *Remote Sensing of Environment*, **62**(3): 201–214 DOI: 10.1016/S0034-4257-(97)00082-5

Jiao Z T. 2008. The use of MODIS BRDF/Albedo Products to recover Land Surface Properties. Beijing: Dissertation of Beijing Normal University: 4–10

Jiao Z T, Wang J D, Xie L O, Zhang H, Yan G J, He L M and Li X W. 2005. Initial validation of MODIS albedo product by using field measurements and airborne multiangular remote sensing observations. *Journal of Remote Sensing*, **9**(1): 64–72

Leroy M and Roujean J L. 1994. Sun and view angle corrections on reflectances derived from NOAA/AVHRR data. *IEEE Transactions on Geoscience and Remote Sensing*, **32**(3): 684–697 DOI: 10.1109/36.297985

Li X W and Wan Z M. 1998. Comments on reciprocity in the BRDF modeling. *Progress in Natural Science in China*, **8**(3): 354–358

Li X W and Strahler A H. 1985. Geometric-optical modelling of a conifer forest canopy. *IEEE Transactions on Geoscience and Remote Sensing*, **23**(5): 705–721 DOI: 10.1109/TGRS.1985.289389

Li X W and Strahler A H. 1986. Geometric-optical bidirectional reflectance modelling of a conifer forest canopy. *IEEE Transactions on Geoscience and Remote Sensing*, **24**(6): 906–919 DOI: 10.1109/TGRS.1986.289706

Liang S L. 2004. Quantitative Remote Sensing of Land Surface. New York: Wiley

Liang S L, Fang H L, Chen M Z, Shuey C J, Walthall C, Daughtry C, Morisette J, Schaaf C B and Strahler A H. 2002. Validating MODIS land surface reflectance and albedo products: methods and preliminary results. *Remote Sensing of Environment*, **83**(1-2): 149–162 DOI: 10.1016/S0034-4257(02)00092-5

Liu J C, Schaaf C, Strahler A, Jiao Z T, Shuai Y M, Zhang Q L, Roman M, Augustine J A and Dutton E G. 2009. Validation of moderate resolution imaging spectroradiometer (MODIS) albedo retrieval algorithm: Dependence of albedo on solar zenith angle. *Journal of Geophysical Research*, **114**: D01106. DOI: 10.1029/2008JD009969

Lucht W, Schaaf C B and Strahler A H. 2000. An algorithm for the retrieval of albedo from space using semiempirical BRDF models. *IEEE Transactions on Geoscience and Remote Sensing*, **38**(2): 977–998 DOI: 10.1109/36.841980

Maignan F, Bréon F M and Lacaze R. 2004. Bidirectional reflectance of Earth targets: Evaluation of analytical models using a large set of spaceborne measurements with emphasis of the hot spot. *Remote Sensing of Environment*, **90**(2): 210–220 DOI: 10.1016/j.rse.2003.12.006

Nicodemus F E, Richmond J C, Hsia J J, Ginsberg I W and Limperis T. 1977. Geometrical Considerations and Nomenclature for Reflectance. NBS Monograph 160. Washington, D.C.: National Bureau of Standards, U.S. Department of Commerce:

Ross J. 1981. The radiation regime and architecture of plant stands. Hague: Dr. W. Junk Publishers:

Roujean J L, Leroy M and Deschamps P Y. 1992. A bi-directional reflectance model of the Earth's surface for the correction of remote sensing data. *Journal of Geophysical Research*, **97**(D18): 20455–20468 DOI: 10.1029/92JD01411

Sandmeier S R and Deering D W. 1999. Structure analysis and classification of boreal forest using airborne hyperspectral BRDF data from ASAS. *Remote Sensing of Environment*, **69**(3): 281–295 DOI: 10.1016/S0034-4257(99)00032-2

Schaaf C B, Gao F, Strahler A H, Lucht W, Li X W, Tsang T, Strugnell N C, Zhang X Y, Jin Y F, Muller J P, Lewis P, Barnsley M, Hobson P, Disney M, Roberts G, Dunderdale M, Doll C, d'Entremont R, Hu B X, Liang S L, Privette J L and Roy D P. 2002. First operational BRDF, albedo and nadir reflectance products from MODIS. *Remote Sensing of Environment*, **83**(1-2): 135–148 DOI: 10.1016/S0034-4257(02)00091-3

Wanner W, Li X and Strahler A H. 1995. On the derivation of kernels for kernel-driven of bidirectional reflectance. *Journal of Geophysical Research*, D**100**: 21077–21089 DOI: 10.1029/95JD02371

Wanner W, Strahler A H, Hu B, Lewis P, Muller J P, Li X, Schaaf C L B and Barnsley M J. 1997. Global retrieval of bidirectional reflectance and albedo over land from EOS MODIS and MISR data: Theory and algorithm. *Journal of Geophysical Research*, **102**(17): 143–161 DOI: 10.1029/96JD03295

Wu A, Li Z and Cilhar J. 1995. Effects of land cover type and greenness on advanced very high resolution radiometer bidirectional reflectances: Analysis and removal. *Journal of Geophysical Research*, **100**(D5): 9179–9192 DOI: 10.1029/95JD00512

Xu X R. 2005. Remote Sensing Physics. Beijing: Peking University Press: 4

Yang H, Li X W and Gao F. 2002. An algorithm for the retrieval of albedo from space using new GO kernel-driven BRDF model. *Journal of Remote Sensing*, **6**(4): 246–251

附中文参考文献

陈永梅，王锦地，梁顺林，王东伟，马斌．2009．MISR和MODIS二向性反射数据产品的对比分析．遥感学报，**13**(5): 808–815

焦子锑．2008．利用MODIS BRDF和反照率产品进行地表特性的研究．北京: 北京师范大学: 4–10

焦子锑，王锦地，谢里欧，张颢，阎广建，何立明，李小文．2005．地面和机载多角度观测数据的反照率反演及对MODIS反照率产品的初步验证．遥感学报，**9**(1): 64–72

徐希孺．2005．遥感物理．北京: 北京大学出版社: 44

杨华，李小文，高峰．2002．新几何光学核驱动BRDF模型反演地表反照率的算法．遥感学报，**6**(4): 246–251

李小文，万正明．1998．互易原理在二向性反射研究中的适用性．自然科学进展，**8**(3): 354–358